MODELLING THE VARIABILITY IN SEISMICALLY INDUCED SLOPE DISPLACEMENTS DUE TO GROUND MOTION SELECTION

A THESIS SUBMITTED TO
THE GRADUATE SCHOOL OF NATURAL AND APPLIED SCIENCES
OF
MIDDLE EAST TECHNICAL UNIVERSITY

BY

BURAK OKAN ÖZMEN

IN PARTIAL FULFILLMENT OF THE REQUIREMENTS
FOR
THE DEGREE OF MASTER OF SCIENCE
IN
CIVIL ENGINEERING

APRIL 2019

Approval of the thesis:

MODELLING THE VARIABILITY IN SEISMICALLY INDUCED SLOPE DISPLACEMENTS DUE TO GROUND MOTION SELECTION

submitted by **BURAK OKAN ÖZMEN** in partial fulfilment of the requirements for the degree of **Master of Science in Civil Engineering Department, Middle East Technical University** by,

Prof. Dr. Halil Kalıpçılar
Dean, Graduate School of **Natural and Applied Sciences** _____

Prof. Dr. Ahmet Türer
Head of Department, **Civil Engineering** _____

Assoc. Prof. Dr. Zeynep Gülerce
Supervisor, **Civil Engineering Dept., METU** _____

Dr. Zeynep Çekinmez Bayram
Co-Supervisor, **Civil Engineering Dept., METU** _____

Examining Committee Members:

Prof. Dr. Kemal Önder Çetin
Civil Engineering Dept., METU _____

Assoc. Prof. Dr. Zeynep Gülerce
Civil Engineering Dept., METU _____

Asst. Prof. Dr. Nejan Huvaj
Civil Engineering Dept., METU _____

Asst. Prof. Dr. Onur Pekcan
Civil Engineering Dept., METU _____

Asst. Prof. Dr. M. Abdullah Sandıkkaya
Civil Engineering Dept., Hacettepe University _____

Date: 03.04.2019

I hereby declare that all information in this document has been obtained and presented in accordance with academic rules and ethical conduct. I also declare that, as required by these rules and conduct, I have fully cited and referenced all material and results that are not original to this work.

Name, Last name: Burak Okan Özmen

Signature:

ABSTRACT

MODELLING THE VARIABILITY IN SEISMICALLY INDUCED SLOPE DISPLACEMENTS DUE TO GROUND MOTION SELECTION

Özmen, Burak Okan
MSc., Department of Civil Engineering
Supervisor: Assoc. Prof. Dr. Zeynep Gülerce
Co-Supervisor: Dr. Zeynep Çekinmez Bayram

April 2019, 73 pages

Assessing the earthquake performance of a slope and estimating the seismically-induced slope displacements is one of the most complicated tasks in geotechnical earthquake engineering. The source of the complication includes: i) defining the soil properties and their variability within the limits of the available geological/geotechnical information, and ii) executing a proper ground motion selection and scaling procedure for the dynamic numerical analysis, which are generally limited in number for most of the engineering applications. The objective of this study is to model the uncertainty due to ground motion selection in the seismically-induced soil slope displacements estimated by the dynamic numerical analysis. For this purpose, fifty horizontal pairs of ground motions recorded at rock stations from the Pacific Earthquake Engineering Research Center database are selected and scaled up to 1.0g of maximum horizontal acceleration to create the candidate ground motion dataset of 300 recordings. These recordings are utilized in PLAXIS-2D software to perform the dynamic numerical analysis for eight different slopes in dry (drained) soil. Analysis results showed that the standard deviation of a simplified prediction model for seismically-induced permanent slope displacements lie within the range of 0.28-0.36 (log units) and does not show a significant variation with factor of safety in static conditions or angle of the slope geometry. At the end of the study, 18 ground motion components that represent the median behaviour are selected and provided for the future studies. These recordings may be preferred in

the numerical dynamic analysis to examine slope displacements and when combined with the estimated standard deviations, the body and the range in seismic demand models for earthquake-induced slope displacements may be properly modelled.

Keywords: Seismically-induced slope displacements, dynamic finite element analysis, ground motion selection and scaling, seismic demand models.

ÖZ

KUVVETLİ YER HAREKETİ SEÇİMİNİN SİSMİK ŞEV DEPLASMANI ÜZERİNDEKİ ETKİSİNİN MODELLENMESİ

Özmen, Burak Okan
Yüksek Lisans, İnşaat Mühendisliği Bölümü
Tez Danışmanı: Doç. Dr. Zeynep Gülerce
Ortak Tez Danışmanı: Dr. Zeynep Çekinmez Bayram

Nisan 2019, 73 sayfa

Dinamik yüklere maruz kalan bir şevin performansının değerlendirilmesi ve deprem-kaynaklı şev deplasmanlarının kestirilmesi, geoteknik deprem mühendisliği uygulamalarının en karmaşıklarından birisidir. Bu uygulamalardaki en kritik noktalar mevcut jeolojik/geoteknik raporların sınırları dahilinde zemin parametrelerinin ve bu parametrelerdeki değişkenliklerin belirlenmesi ve mühendislik uygulamalarının çoğu için dinamik analiz sayısının sınırlı olmasından dolayı uygun yer hareketi seçimi ve ölçeklendirme işleminin yapılmasıdır. Bu çalışmanın amacı, sonlu elemanlar yöntemi ile yapılan dinamik analizlerde elde edilen deprem-kaynaklı şev deplasmanlarının, kuvvetli yer hareketi seçimine bağlı değişkenliğinin modellenmesidir. Bu amaçla, Pasifik Deprem Mühendisliği Araştırma Dairesi veri tabanından kayaya oturtulmuş istasyonlarda ölçülmüş 50 adet kuvvetli yer hareketi yatay çifti seçilmiş ve 1.0g maksimum yer ivmesine kadar ölçeklendirilerek 300 adet aday kayıt içeren bir veriseti hazırlanmıştır. Seçilen yer hareketi kayıtları kullanılarak, şev deplasmanlarını belirlemek için PLAXIS 2D yazılımı aracılığıyla sekiz farklı kuru (drenajlı) zemin için belirlenen şev geometrisi analiz edilmiştir. Analiz sonuçlarına göre oluşturulan basitleştirilmiş deprem kaynaklı şev deplasmanlarını tahmin modelinin standart sapması 0.28 ile 0.36 arasında değişmektedir ve bu değer statik güvenlik katsayısı veya şev açısına bağlı olarak fazla değişim göstermemektedir. Çalışma sonunda, gelecekteki deprem kaynaklı şev deplasmanlarının belirlenmesinde kullanılabilecek, ortalama davranışı temsil eden 18

adet kuvvetli yer hareketi yatay bileşeni seçilmiştir. Numerik dinamik analizlerde bu kayıtların tercih edilmesi ve önerilen standart sapma ile birleştirilmesi halinde, tahmin modellerinin merkezinin ve dağılımının doğru bir biçimde temsil edilmesi mümkün olacaktır.

Anahtar Kelimeler: Deprem kaynaklı şev deplasmanlarını, dinamik sonlu elemanlar analizi, kuvvetli yer hareketi seçimi ve ölçeklendirilmesi, sismik talep modeli.

To My Family

ACKNOWLEDGMENTS

I would like to express my deepest gratitude to my supervisor Assoc. Prof. Dr. Zeynep Gülerce for her patience, guidance, criticism and encouragement throughout the research.

I am grateful to my co-supervisor Dr. Zeynep Çekinmez Bayram for significant discussions and her advices on my study.

I especially would like to thank Burak Akbaş. I believe this thesis would not be completed without his contributions.

Finally, my biggest gratitude is for my beloved family. I would like to thank my mother Şerife Özmen, my father Mesut Özmen and my sister Hatice Özmen for their endless love and support.

TABLE OF CONTENTS

LIST OF TABLES

TABLES

LIST OF FIGURES

FIGURES

CHAPTER 1

INTRODUCTION

Landslides are one of the principal causes of damage during earthquakes; the amount of damage from seismically induced landslides and other ground failures sometimes exceed the amount of damage that is directly related to ground shaking and fault rupture (Refice and Capalongo, 2002). The 2008 Wenchuan Earthquake is by far the largest event in the last century in terms of the number and volume of earthquake-induced landslides (Figure 1.1a) and the affected area (Fan et al., 2018), leading to several papers published on various aspects of seismically-triggered landslides (Tanyaş, 2019). However, most of the previous literature (both before and after the Wenchuan Earthquake) focused on documenting the case histories in terms of the spatial properties of the earthquake-induced landslides and their relation with geological and geomorphological indices, analysed the earthquake or ground motion parameters that may trigger the landslides, evaluated or developed landslide susceptibility maps, etc. During the recent Nepal-Gorkha Earthquake (2015), landslides covering more than 90 km^2 of area were triggered (Martha et al., 2017, Figure 1.1b) and the collected data significantly challenged the previously developed prediction models for estimating the volume and spatial distribution of seismically induced landslides (Tanyaş, 2019). Therefore, it would be safe to assume that the future studies based on landslide susceptibility mapping and remote sensing will focus on further developing the landslide inventories and improving the prediction models for spatial distribution of seismically induced landslides.

For the geotechnical engineering point of view, the ability to predict seismically-triggered landslide displacements due to expected ground shaking levels and general slope properties is more important, especially for the analysis of geotechnical hazards and for the design of engineering slopes (Jibson, 1993). Jibson (2011)

grouped the dynamic (seismically induced) slope stability analysis methods under three main headings: the pseudo-static analysis, stress-deformation analysis, and permanent displacement analysis. Using the same main headings, previous literature with the advantages and limitations are discussed in **Chapter 2** of this dissertation. Considering the seismically-triggered permanent slope displacement as the seismic performance parameter (or the engineering demand parameter, EDP), several prediction models (also known as seismic demand models) based on different ground motion intensity measures (IMs) were developed over the last two decades. Almost all of the previous seismic demand models had utilized the Newmark's sliding block (NSB) analogy to calculate the permanent slope displacement. The performance and the applicability of recent prediction models for NSB displacement in Turkey were evaluated and discussed by Gülerce and Balal (2017); therefore, these models are not included in the scope of this study. For other slope failure types, the use of stress – strain/displacement methods is getting more widespread since complex slope geometries and different large-strain soil models can be incorporated in these analysis. Permanent slope displacement prediction models based on dynamic numerical analyses are quite limited: only a few studies were published over the last decade and the findings of these studies are summarized in Chapter 2.

(a) (b)

Figure 1.1 (a) Earthquake-induced slope failure of a natural slope in 2008 Wenchuan Earthquake (source: sciencedaily.com), (b) failure of a natural slope after the 2015 Nepal-Gorkha Earthquake caught on camera ((source: indianexpress.com)

Previous literature given in Chapter 2 displayed that the uncertainties in the input ground motion used for the NSB displacement prediction models were only recently addressed in the literature (e.g. Rathje and Saygili (2008), Strenk and Wartman (2011)). Strenk and Wartman (2011) showed that the uncertainty in the input motion may have a significant effect on the slope displacement estimates and the amplitude of the effect depends on the applied methodology (NSB or decoupled analysis). However, a comprehensive evaluation of the uncertainty implied by the ground motion selection on the results of stress-deformation analysis for slope displacement was not provided in any of the previous works.

1.1 Objective and Scope

The fundamental objective of this study is to model the variability in the earthquake-induced permanent slope displacements estimated by dynamic numerical analysis due to the selection of the input ground motion. For this purpose, fifty horizontal pairs of ground motions recorded at rock stations from the Pacific Earthquake Engineering Research Center (PEER) Next Generation Attenuation West 2 database are selected and scaled up to 1.0g of maximum horizontal acceleration to create the candidate ground motion dataset of 300 recordings. These candidate recordings are utilized in PLAXIS-2D software to perform the dynamic numerical analysis for eight different slopes in dry (drained) soil with different slope geometries. At the beginning of **Chapter 3**, the procedures developed for the selection and scaling of input ground motions are defined. Additionally, details regarding the utilized slope geometries and geotechnical parameters are elaborated in that chapter.

Analysis results provided in **Chapter 4** shows that the relationship between the permanent slope displacements and peak ground acceleration (PGA) of the input motion is linear in log space. For the scope of this study, the scatter or the standard deviation of the relationship is more important; therefore, the variation of the standard deviation with the slope parameters (i.e., factor of safety in static condition or slope angle) is discussed in **Chapter 5**. Analysis results showed that the standard deviation of a simplified prediction model lie within the range of 0.28-0.36 (log units) and does not show a significant variation with factor of safety in static

conditions or angle of the slope geometry. The final objective of this study is to choose a small set of ground motions that captures the median relationship between the permanent slope displacement and PGA for the future studies. These recordings may be preferred in the numerical dynamic analysis to examine slope displacements and when combined with the estimated standard deviations, the body and the range in seismic demand models for earthquake-induced slope displacement may be properly modelled.

CHAPTER 2

LITERATURE REVIEW

Since the beginning of the twentieth century, a variety of methods had been developed to investigate earthquake-related slope stability. According to Jibson (2011), these methods can be grouped under three main groups with an increasing order of the complexity and expense as: (1) pseudostatic analysis, (2) Newmark sliding block analysis and its derivatives, and (3) stress-deformation analysis.

2.1 Pseudostatic Analysis

Pseudostatic analysis method is one of the oldest seismic slope stability analysis methods that is still in use today. Although pseudostatic method was developed based on earlier works, it was first introduced by Terzaghi (1950). In this method, earthquake loads are considered as a constant force, which is assumed to directly act as a single force to the centre of gravity of the sliding mass. Then the safety factor of the slope is calculated with the limit equilibrium formula. Horizontal seismic loads increase in proportion to the weight of the sliding mass (W) and the pseudo static coefficient (k) and they are applied to slope as shown in Figure 2.1. The pseudo static coefficient is defined in Equation 1:

$$k = \frac{a_h}{g} \qquad \text{(Eq. 1)}$$

where a_h the horizontal acceleration of the strong ground motion and g is the acceleration of gravity. The general method in the analysis is to carry out iterative limit equilibrium analyses with variable k values to find a pseudo static coefficient value that makes factor of safety equal to one. Obtained pseudostatic coefficient is

named as the yield coefficient (α_y) and it is assumed that the slope will become unsafe if the horizontal earthquake recording acceleration exceeds the α_y value.

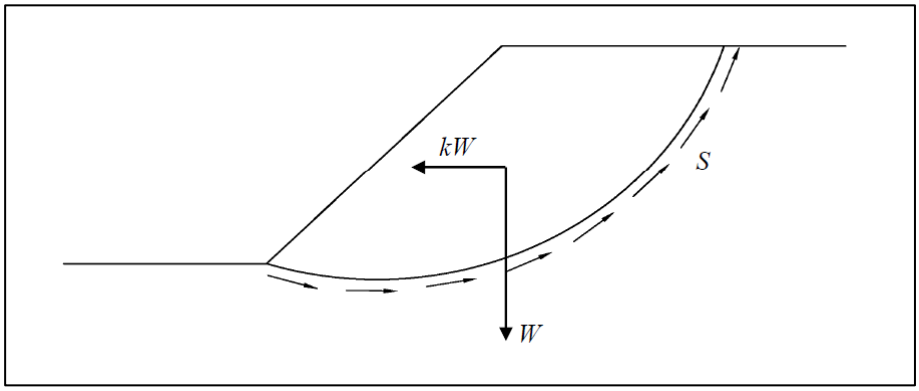

Figure 2.1 A simplified sketch of pseudostatic slope stability analysis

Although the method of pseudostatic analysis is quite simple and easy to apply, there are disadvantages and assumptions that are incompatible with the reality. One of these disadvantages is that pseudostatic method performs static analyses by assuming that the earthquake loads are constant and unidirectional. However, seismic loads like earthquakes continuously change direction and quantity. Another weakness of the pseudo static analysis is that it does not provide information about plastic slope displacement occurred during the seismic loading. In other words, the slope stability is evaluated in pseudostatic analysis, but the method cannot provide any information about the amount of motion of the sliding mass after the limit balance has been exceeded. In most cases, if the factor of safety falls below of one, it is assumed that the sliding mass is completely failed. For these reasons, Stewart et al. (2003) recommended that pseudostatic analysis should be used only for preliminary designs and should be followed by more advanced analysis, because pseudostatic analysis only provides a very rough approximation of slope behaviour during earthquake shaking.

2.2 Newmark Sliding Block Analysis and Its Derivatives

As mentioned previously, the pseudostatic analysis method only provides information about the slope strength against earthquake as factor of safety, but does not provide any information about the amount of permanent displacements occurred during the earthquake. However, serviceability of a slope depends on the amount of

plastic displacement generated during the earthquake. For this reason, analyses that predict slope displacement provide a more useful data for seismic slope stability.

In the method introduced by Newmark (1965), pseudostatic analysis approach had taken one-step forward and slope displacements were incorporated in the calculations with the help of acceleration time history of the ground motion. In this method, acceleration time history of selected ground motion is compared with the yield acceleration value to calculate the slope displacements, (Abramson et al., 2002). In the Newmark rigid block analysis method, it is assumed that the moving soil mass behave as a single rigid block which is sliding over an inclined plane. This analogy is shown in Figure 2.2. The seismically induced slope displacements are estimated by displacement of the rigid block sliding along inclined plane under the influence of earthquake acceleration.

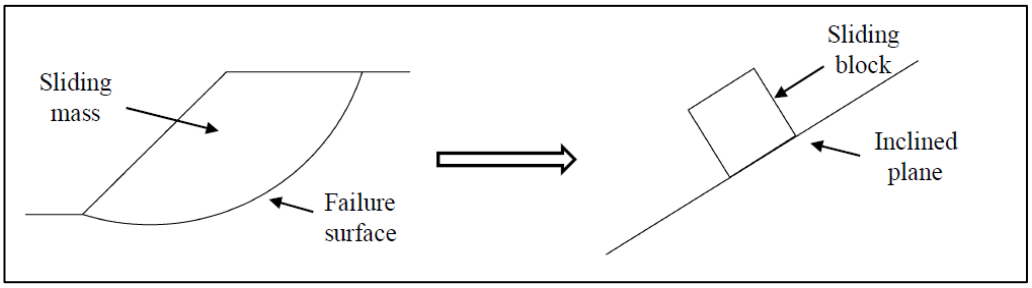

Figure 2.2 Demonstration of Newmark's sliding block analyses

Figure 2.3 shows the simple expression of Newmark rigid block analyses. Figure 2.3(a) shows an acceleration time history and a dashed line refers to the yield acceleration value (a_y), which can be determined as mentioned pseudostatic analyses. The plastic displacements occur when the ground motion acceleration exceeds the yield acceleration, which is indicated by the shaded areas. These shaded areas are integrated as a function of time to obtain velocity time history as shown in the Figure 2.3(b). Similarly, the displacement-time graph is obtained by integrating the velocity-time graph as a function of time as shown in Figure 2.3(c). Therefore, the displacement amount of the sliding mass is obtained by taking the double integral of the portions of acceleration-time graph that exceeds the yield acceleration. If the peak ground acceleration (PGA) is less than the yield acceleration, no displacement will occur.

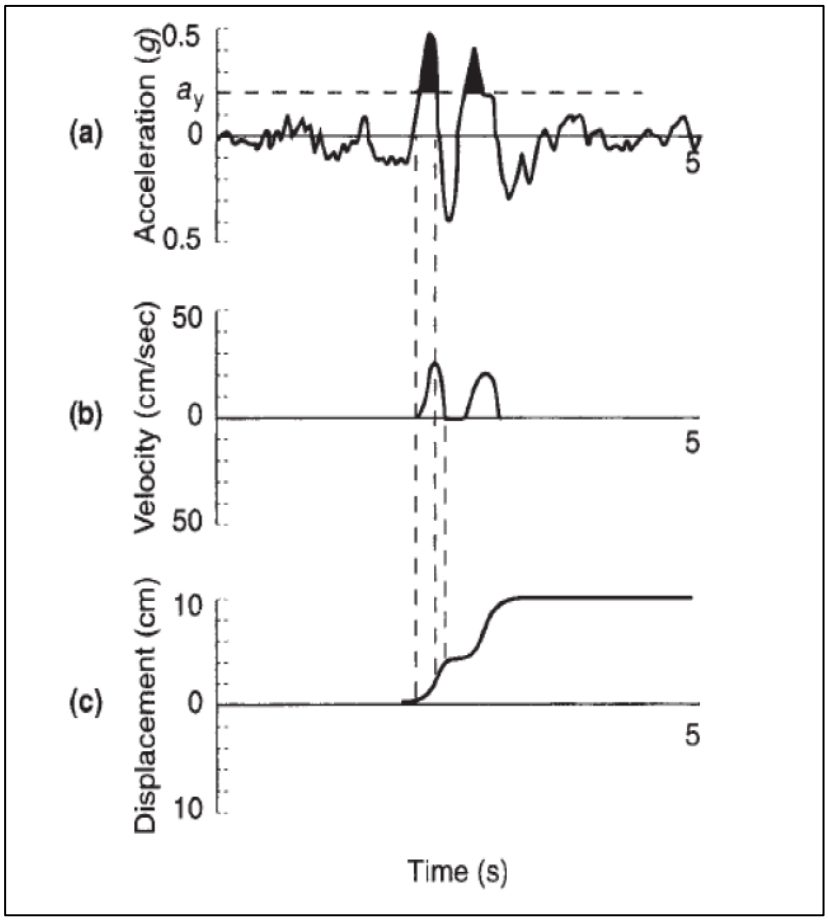

Figure 2.3 Illustration of the Newmark sliding block method calculation steps: (a) acceleration time history, (b) velocity time history, (c) displacement time history (Wilson and Keefer, 1985)

One of the most important advantages of the Newmark rigid block analysis is that it is simple and practical. However, these properties are due to the many assumptions that affect the accuracy of the obtained results. First, it is assumed that sliding mass acts as a single rigid block and shows no inner displacement during sliding. Moreover, it is expected that sliding will occur only when the ground acceleration exceeds yield acceleration value. However, in reality soils rarely show perfectly plastic material behaviour, instead they usually exhibit strain hardening or softening with increasing strains. As a result, the yield acceleration value is expected to increase with increasing displacements and the changing geometry of the moving mass (Kramer, 1996).

Various arrangements have been made to Newmark sliding block procedure to obtain more accurate results of seismically induced slope displacements by modelling the

slopes in a more realistic way. Makdisi and Seed (1978) improved the Newmark sliding block method to include the displacements occurred in the sliding mass during seismic loading. This method was named as decoupled method because the dynamic response of sliding mass and plastic slope displacement were calculated separately in two steps. As a first step, a dynamic response analysis computed to obtain the average accelerations experienced by the slide mass. For this step, it is necessary to specify the shear wave velocity of sliding mass, thickness of potential slide, modulus reduction curve and damping ratio of soil. The second step, to calculate the amount of displacement Newmark double integration method, as mentioned previously, was used with the average acceleration time history as input motion.

Lin and Whitman (1983) pointed out that the effects of slip on the ground are not taken into consideration in the decoupled analyses method and they suggested coupled analyses that reflect the real slope behaviour in a better way. The dynamic response of the sliding mass and the permanent displacement, which is calculated separately in the decoupled method, are modelled together in coupled method. In the analysis, it is required to specify the shear wave velocity of the materials above and below the slip surface and their thickness, modulus reduction curve, damping ratio of potential landslide. The sliding effects on the dynamic system are accounted for by introducing the sliding force at the sliding interface into the dynamic motions.

2.3 Stress Deformation Analysis

The above-mentioned analytical methods can generally be used with simplified geometry and model and are not reliable in simulating complex geological conditions and soil behaviour (e.g., hardening or softening of soil, topography, soil profile and seismic shaking). In order to overcome these limitations, stress deformation computational techniques such as finite element method (FEM) and finite difference method (FDM) were developed. These methods have been used to predict displacements of slopes caused by seismic loading (Seed et al., 1973; Griffiths and Prevost, 1988; Elgamal et al., 1990). FEM and FDM analyses divides the whole domain into deformable sub-domains (i.e. mesh) which are connected to each other

with points called “nodes” and then calculates the deformation and stress change at each node.

The advantage of stress deformation models is that they can simulate the real situation very accurately. Another advantage of stress deformation models is that they can be overcome the complex topographic condition and imitate the complex soil behaviour more realistically. Moreover, these methods can give a better idea about the mechanism of the earthquake induced slope displacements, especially the progressive movement of seismic slope failure. Clearly, models that account for the complexity of variability of material properties and the stress-strain behaviour give results that are more reliable. However, stress-deformation modelling has also a disadvantage. The models are not able to work with large displacements due to the limitation of mesh size.

According to finite element method, a continuum is divided into a number of (volume) elements. Each element, which may be one, two or three dimensions, consists of a number of nodes and is connected to each other only at their nodes. Displacements may be resulted due to the self-weight of the elements or the external loads.

2.3.1 Software Finite Element Analyses Using PLAXIS 2D

In geotechnical engineering, obtaining the exact solution is a challenging issue. However, using a numerical modelling, approximate solutions can be achieved. Problem geometry is divided into smaller elements (i.e., meshes) so that finite elements matrix at the nodes can be obtained in order to approach the solution. In one of the special case for FEM, problem can be modelled in 2D if plane-strain conditions are valid. In this study, the problem of permanent slope displacement under seismic loading can be analysed under 2D plane-strain conditions. In order to achieve this goal, software called PLAXIS 2D is utilized. One of the crucial aspect of this approach is to select the most appropriate soil model that can accurately simulate the real-life behaviour of the site.

Another aspect of this method is to choose the element type. Among the available elements in PLAXIS 2D, in order to increase the accuracy, 15-noded triangular elements are utilized. These elements contain 12 stress points and 15 nodes for the calculations (Figure 2.4).

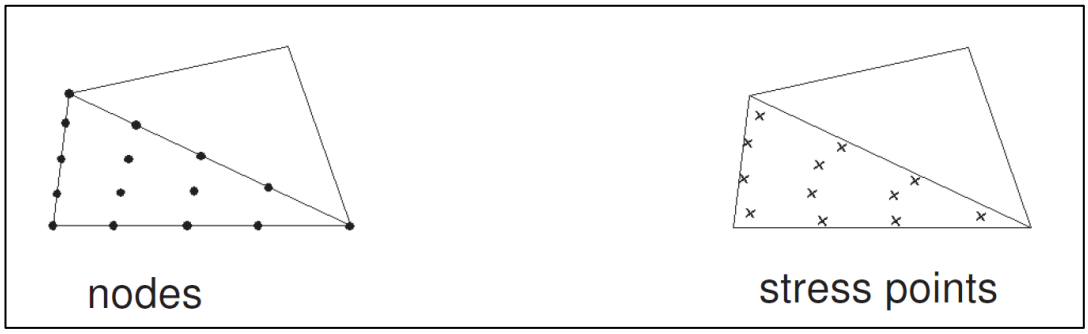

Figure 2.4 Example of nodes and stress points positions in mesh element (PLAXIS 2D Reference Manual, 2016)

In this study, phi/c reduction (safety) analysis and dynamic analysis options are used. First option is used in order to determine static factor of safety values of slopes whereas second option is utilized for the calculation of earthquake-induced displacements. In next section, material model used in the analyses are explained briefly since the selection of the appropriate model is crucial in order to simulate the complex, non-linear soil behaviour.

2.3.1.1 The Hardening Soil Model and The Hardening Soil Model with Small-Strain Stiffness

In this study for dynamic analyses, Hardening Soil Model with Small-Strain Stiffness (HSSMALL) which is the modified version of Hardening Soil Model (HSM) is utilized for the simulation of appropriate soil behaviour. Hence, these material models are briefly explained in this section. Selection of the material model is crucial for the accuracy of the results. As stated by PLAXIS 2D Material Models Manuals (2016), different soil types can be simulated by using HSM in order to capture the nonlinear and inelastic stress-strain behaviour for both soft and stiff soils. This model was developed based on Duncan-Chang model which is also known as the hyperbolic model (Duncan and Chang, 1970; PLAXIS 2D Material Models Manuals, 2016). One of the basic features of this model is its stress-dependent soil stiffness

property with the help of soil parameters such as unloading-reloading modulus, E_{ur}. Required parameters for this model are: cohesion, c, internal friction angle, ϕ, dilatancy angle, ψ, secant stiffness in standard drained triaxial test, $E_{50,}$ tangent stiffness for primary oedometer loading, E_{oed} ,unloading-reloading stiffness, $E_{ur,}$ power for stress-level dependency of stiffness, m

Since Duncan-Chang model uses theory of elasticity but HSM uses theory of plasticity, HSM surpasses the Duncan-Chang model for the simulation of unloading/reloading behaviour. Basis of HSM contains hyperbolic relation between ε_a (axial strain) and q (deviatoric stress) as given Equation 2:

$$-\varepsilon_1 = \frac{1}{E_i}\frac{q}{1-q/q_a} \qquad for\ q < q_f \qquad \text{Eq. (2)}$$

where; q_a is the asymptotic value of the shear strength whereas E_i is the initial stiffness. E_i can be expressed as given Equation 3

$$E_i = \frac{2E_{50}}{2-R_f} \qquad \text{Eq. (3)}$$

where; E_{50} is confining stress dependent stiffness for primary loading and it can be expressed as given Equation 4:

$$E_{50} = E_{50}^{ref}\left(\frac{ccos\phi-\sigma_3' sin\phi}{ccos\phi+p^{ref}sin\phi}\right)^m \qquad \text{Eq. (4)}$$

Where; E_{50}^{ref} is a reference stiffness modulus corresponding to reference confining stress of p^{ref} which is in taken as 100 kPa in PLAXIS 2D. Additionally, power m represents the stress dependency of the soil.

Ultimate deviatoric stress (q_f) and asymptotic value of the shear strength (q_a) can be shown as given Equation 5 and Equation 6 respectively:

$$q_f = (ccot\phi - \sigma_3')\frac{2sin\phi}{1-sin\phi} \qquad \text{Eq. (5)}$$

$$q_a = \frac{q_f}{R_f}$$ Eq. (6)

In PLAXIS 2D, R_f is taken as 0.9 by default.

Finally, unloading-reloading path can be simulated using an appropriate stiffness that can be expressed as given Equation 7:

$$E_{ur} = E_{ur}^{ref} \left(\frac{ccos\phi - \sigma_3' sin\phi}{ccos\phi + p^{ref} sin\phi}\right)^m$$ Eq. (7)

Where; E_{ur}^{ref} is the reference Young's modulus for unloading-reloading path corresponding to p^{ref}.

Nonlinear dependency on the strain level of the soil's shear modulus even for the small-strain levels should be considered in dynamic analyses. Therefore, while integrating 2 additional parameters, HSSMALL model can consider nonlinear soil stiffness decay in the analyses at small strain levels. Required additional parameters for HSSMALL are; small-strain shear modulus, G_0, shear strain level ($\gamma_{0.7}$) at which the secant shear modulus G_s is reduced to 70% of G_0

By using these additional parameters and hyperbolic law proposed by Hardin-Drnevich relationship, stress-strain curve can be obtained (PLAXIS 2D Material Models Manual, 2016). Additionally, Santos and Correia (2001) modified this relationship (Figure 2.5) and PLAXIS 2D uses the modified relation for the shear modulus degradation.

Santos and Correia (2001) relationship between G_s and G_0 can also be expressed as given Equation 8:

$$\frac{G_s}{G_0} = \frac{1}{1+0.385*\left|\frac{\gamma}{\gamma_{0.7}}\right|}$$ Eq. (8)

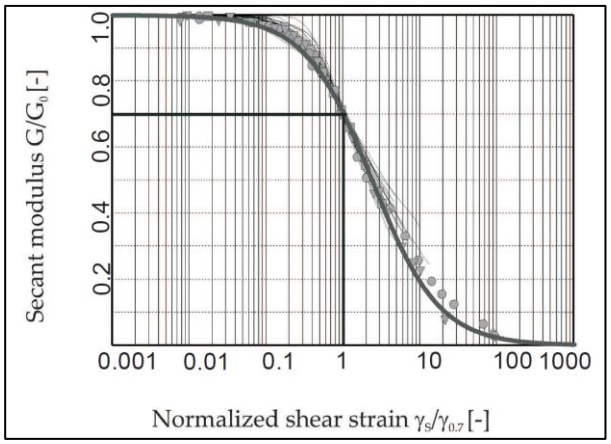

Figure 2.5 Comparison between Hardin-Drnevich relationship and Santos and Correia (2001) test data (PLAXIS 2D Material Models Manual, 2016)

Relationship between tangent modulus and G_0 is also provided given in Equation 9:

$$\frac{G_t}{G_0} = \frac{1}{\left(1+0.385*\frac{\gamma}{\gamma_{0.7}}\right)^2} \quad \text{Eq. (9)}$$

Finally, as it is the case for the HSM model, stress dependency of G_0 can be expressed as Equation 10:

$$G_0 = G_0^{ref}\left(\frac{c\cos\phi-\sigma_3'\sin\phi}{c\cos\phi+p^{ref}\sin\phi}\right)^m \quad \text{Eq. (10)}$$

In HSSMALL material model, under the cyclic loading, as the shear stiffness degrades, soil exhibits hysteric damping. This hysteric behaviour is provided in Figure 2.6. Formulation of this damping is given in Equation 11:

$$\xi = \frac{E_D}{4\pi E_S} \quad \text{Eq. (11)}$$

where; E_D and E_S (energy stored at maximum strain, γ_c) can be expressed as Equation 12 and Equation 13 respectively;

$$E_D = \frac{4G_0\gamma_{0.7}}{0.385}\left(2\gamma - \frac{\gamma_c}{1+\gamma_{0.7}/0.385\gamma_c} - \frac{2\gamma_{0.7}}{0.385}ln\left(1+\frac{0.385\gamma_c}{\gamma_{0.7}}\right)\right) \quad \text{Eq. (12)}$$

$$E_S = \frac{1}{2}G_S\gamma_c^2 \quad \text{Eq. (13)}$$

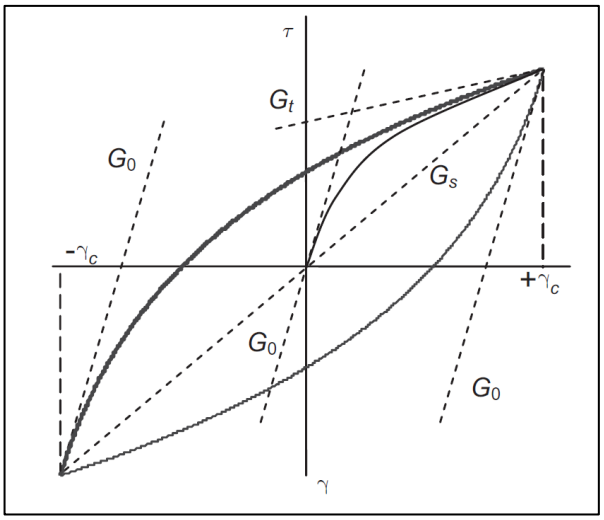

Figure 2.6 Hysteric Behaviour in HSSMALL (Brinkgreve et al., 2007)

Since HSSMALL model can overcome the shortcomings of HSM model in dynamic applications, HSSMALL material model is selected for the analyses as suggested by PLAXIS 2D Material Models Manual (2016).

2.3.1.2 Boundary Conditions

In the dynamic analyses, in order to simulate the real-life soil behaviour, certain type of boundaries different from standard boundaries should be used. One of them is the required boundaries at the right and left sides of the model. In order to imitate the wave propagation that would be the case in real life, boundaries called as “free field” are used for these lateral edges. This boundary enables the waves to propagate as if the model sides are infinite. In other words, wave reflections are, if not completely eliminated, minimized when they hit the model boundaries.

In free field boundary elements, dashpot system is available in both horizontal and vertical directions at every node of the model (Figure 2.7). These dashpot systems equate the normal and shear force coming from the meshes of the model. Free field boundaries are generally preferred for the earthquake analysis in which the main input is the acceleration-time histories. This boundary condition is suggested by the PLAXIS 2D Reference Manual as well as adopted for many researchers (Cundall et al., 1980; Dutta and Roy, 2002; Spyrakos et al., 2009; Xu and Fatahi, 2018).

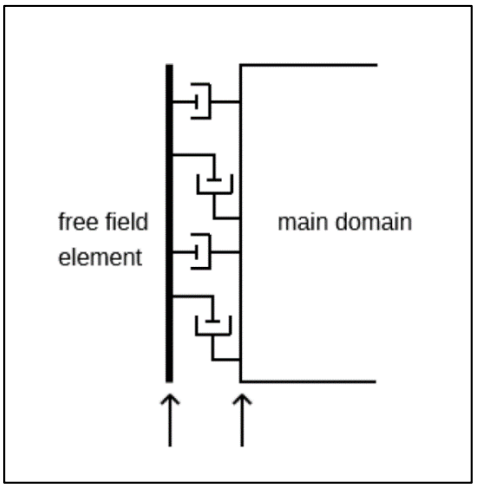

Figure 2.7 Free Field Boundary Condition (PLAXIS 2D reference manual)

Another type of boundary required for the dynamic analyses is called as “none” in PLAXIS 2D. Adopted name of this boundary changes from sources to sources or software to software but main idea behind this boundary is to simulate the engineering bedrock which is very rigid in real life. This boundary creates a scenario in which a very rigid bottom layer and a relatively softer layer on top of it. Additionally, with the help of this boundary condition, line prescribed displacement can be applied to the model base in order to imitate the earthquake motion. As opposed to the “free field” boundaries, this boundary enables a full reflection (PLAXIS 2D Reference Manual).

2.3.1.3 Selection of the Time Step

Suitable time step should be selected in order to increase reliability of the dynamic analyses. If the time step is too large, calculated values could be unreliable and deviated from the actual value. This can be assured in the PLAXIS 2D using the critical time step calculations. In other words, software determines the critical time step value and optimizes the necessary time steps accordingly. This time step is also chosen to ensure that a wave during a single step does not move a distance larger than the minimum dimension of an element. This critical value depends on the largest dimension of the finite elements, area of the finite element, Poisson’s ratio, the average element length, Young’s modulus and density of the material and also the time history function used in calculation.

2.3.1.4 Safety Calculation

In order to compute static factor of safety, strength reduction method (c/phi reduction) was used. In this method, the shear strength parameters (i.e., tanϕ and cohesion) of the soil are systematically reduced in small increments until failure of soil mass occurs. The obtained strength reduction factor, SRF, is comparable with the commonly used static factor of safety and defined as Equation 14.

$$\mathrm{SRF} = \mathrm{FS} = \frac{\tan\phi_{\mathrm{input}}}{\tan\phi_{\mathrm{reduced}}} = \frac{c_{\mathrm{input}}}{c_{\mathrm{reduced}}} = \frac{\mathrm{Strength}_{\mathrm{input}}}{\mathrm{Strength}_{\mathrm{reduced}}} \qquad \text{Eq. (14)}$$

where, the strength parameters with the subscript "input" refer to the initial values in whereas the parameters with the subscript "reduced" refer to the reduced values in the final stage.

2.4 Previous Literature on the Uncertainty in Slope Displacement Models

The objective of the study by Watson-Lamprey and Abrahamson (2006) was to propose a ground motion selection procedure that leads to near average response of a complicated non-linear system using a simple non-linear model as proxy. The simple non-linear proxy was selected as the Newmark's sliding block (NSB) analyses. The NSB displacement prediction model proposed by Watson-Lamprey and Abrahamson (2006) was derived using the PEER NGA-W1 database that contains 3079 ground motion pairs from 175 earthquakes. None of the recordings in the PEER NGA-W1 database was eliminated and all recordings were scaled by seven different scale factors (0.5, 1, 2, 4, 8, 16 and 20). NSB displacements of these scaled recordings were computed for three yield accelerations (0.1g, 0.2g and 0.3g). The standard deviations of NSB displacement model residuals varied between 0.56 and 0.42 in Ln units and they decrease with increasing scale factor according to Figure 2.8. The standard deviation of the proposed slope displacement prediction equation was low compared to other models discussed below, since four different ground motion IMs were used in the models. Watson-Lamprey and Abrahamson (2006) concluded that there is no fundamental problem in using big scale factors for input ground motions.

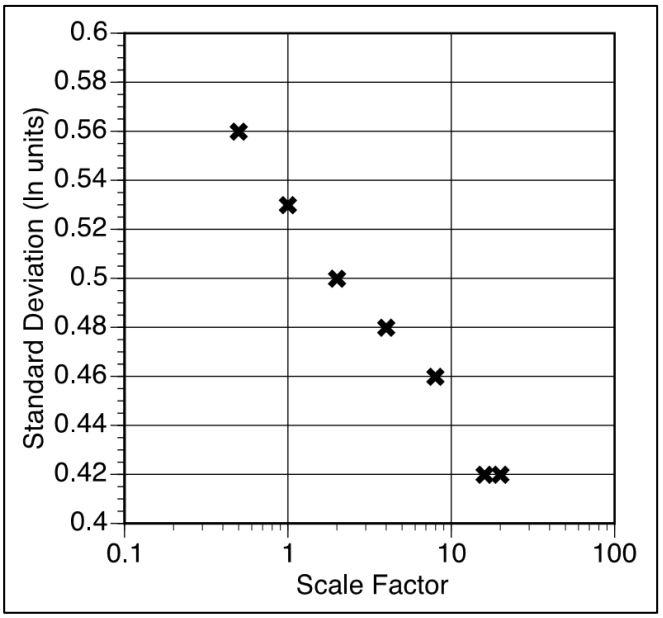

Figure 2.8 Variation of the standard deviation of proposed model with scale factor

Saygılı and Rathje (2008) proposed both scalar and vector-valued predictive models for earthquake induced sliding displacements of slopes. Their subset of PEER NGA-W1 database included the ground motions from earthquakes with M_w=5-7.9 that were recorded up to 100km distances. Ground motions recorded on soft sites or lied outside the corner frequencies of 0.25Hz to 10Hz were eliminated from the data set, resulting in 2383 candidate ground motions. Approximately 25% of the ground motions were too small to result in a positive NSB displacement; therefore, remaining ground motions were scaled by 2.0 and 3.0 to increase the number of analyses. During scaling, the ground motions were capped at PGA=1.0g to ensure that unreasonable PGA values were not created. The slope displacements were calculated using the NSB analogy.

Computed NSB displacement values were used to develop the prediction equations as a function of k_y and different combinations of ground motion IMs (PGA, PGV, mean period, I_a). Saygılı and Rathje (2008) proposed that when PGA was utilized as a single ground motion IM, the standard deviation of the model was found as 1.20 in Ln units. Based on their ability to significantly reduce the standard deviation for the NSB displacement prediction, the two-IM vector-valued model (PGA, PGV) and the three-IM vector-valued model (PGA, PGV, I_a) were recommended by the authors. Standard deviations of the equation for two-IM models are changing between 0.44 to

0.88 based on k_y/PGA ratio. Likewise, standard deviations of the equation for three-IM models are changing 0.25 to 0.92 as shown in the Figure 2.9.

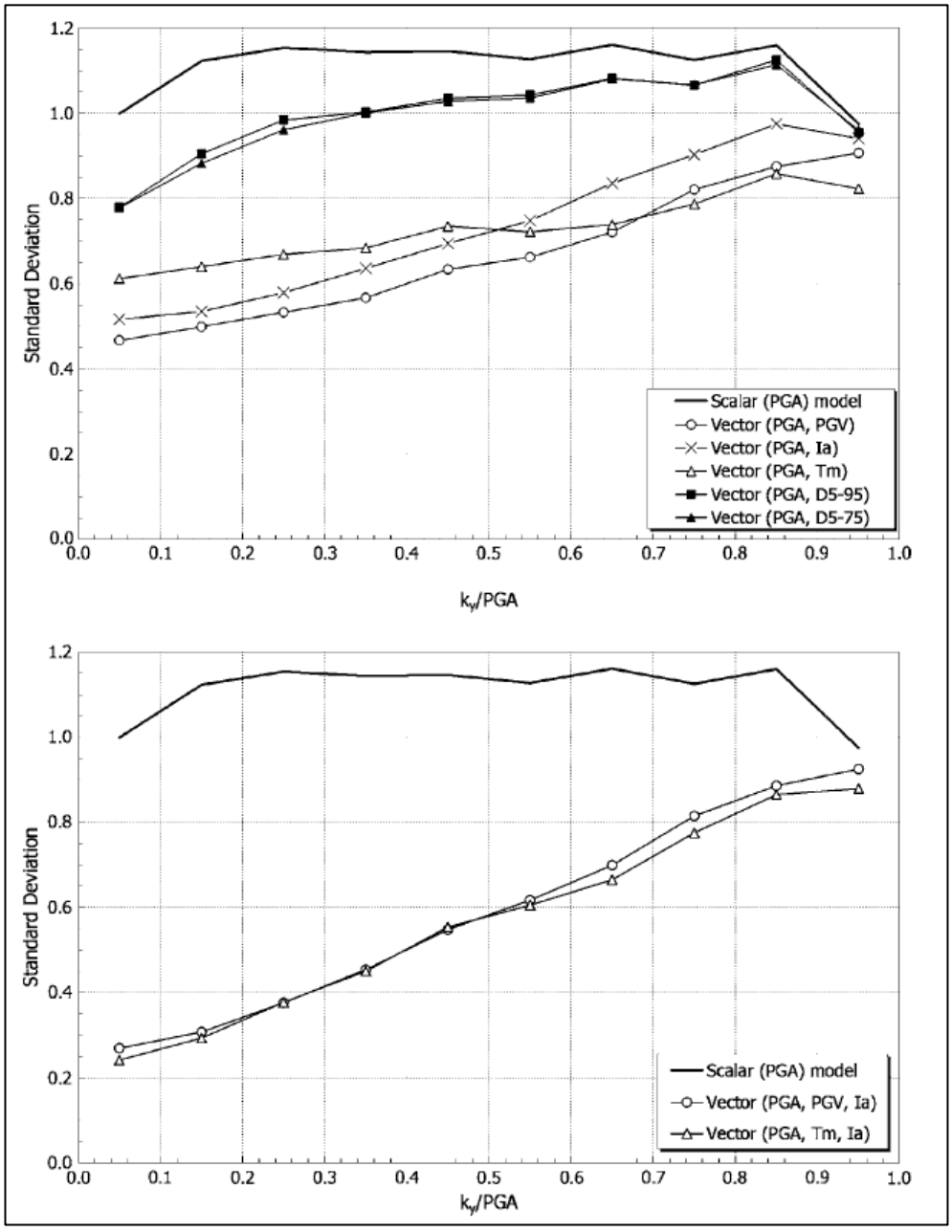

Figure 2.9 Variation of standard deviation with k_y/PGA for (a) scalar and two parameter IM models and (b) three parameter IM models proposed by Saygılı and Rathje (2008)

Strenk and Wartman (2011) used two idealized slope geometries in the analyses as shown Figure 2.10: The shallow failure surface represents a translational slide and the deep failure surface represents the block movement. The scenario earthquake used in that study was the 1994 Northridge earthquake (M_w=6.7) and the rupture

distance was considered as 9.4 km. Based on this scenario, predictions of the Abrahamson and Silva (2008) attenuation relationship were utilized to develop the target spectra that represent the median ±3 standard deviations. Because the scope of this study was the Northridge event, four ground motions from this earthquake was selected. The target spectra and the selected ground motions were randomly paired and different input motions were created using spectral matching (Figure 2.11).

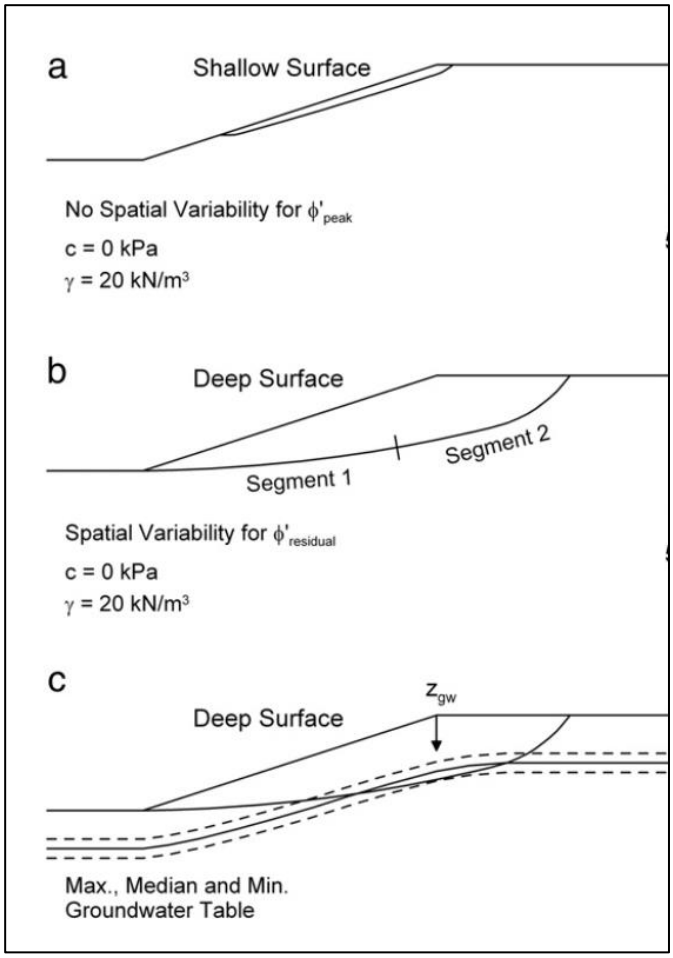

Figure 2.10 Slope geometries used in analyses by Strenk and Wartman (2011)

Generated slope geometries and input ground motions were combined in FLAC software to estimate the slope displacements. As a result, high levels of predictive uncertainty were determined in slope displacements and this uncertainty was related with the non-linearities in the sliding block type models and the inherent variability in input ground motions. Strenk and Wartman (2011) also proposed that predictive uncertainty is a function of slope's relative degree of stability, with low acceleration ratios yielding greater displacement uncertainty than higher acceleration ratios.

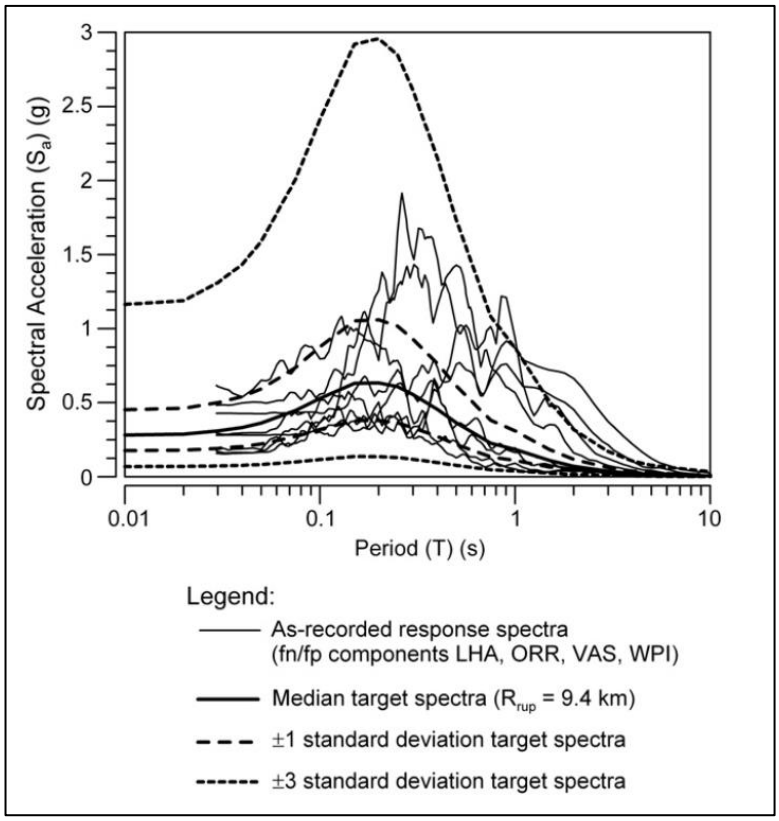

Figure 2.11 The ground motions and the target spectra used by Strenk and Wartman (2011)

Fotopoulo and Pitilakis (2015) proposed series of prediction equations for earthquake-induced slope displacements based on the results of numerical analyses. They studied 12 different slope configurations by changing slope inclination, slope height and strength parameters as seen in the Figure 2.12 using finite difference analyses performed in FLAC 2D. In the analyses, 40 different real acceleration-time histories selected from Seismic Hazard Harmonization in Europe (SHARE, www.share-eu.org) database utilized. During the record selection procedure, the ground motions recorded on rock outcrop were preferred. Selected ground motions have M_w range of 5-7.62, epicentral distances of 3.4-71.4 km, $V_{s,30}$ range of 602-2016 m/s, PGA range of 0.065-0.91g and PGV range of 3.1-78.5 cm/s. In this study, free-field boundaries and Mohr-Coulomb material model were used. They assigned mass and stiffness-proportional Rayleigh damping as 3% for the soil layers and 0.5% for the elastic bedrock. At the end of the analyses, 285 nonzero maximum slope displacements were estimated and the slope displacements for the prediction models were calculated by multiplying the maximum displacements by 0.65. The reduced

maximum slope displacements calculated by Fotopoulo and Pitilakis (2015) reached up to 1.0 m as shown in Figure 2.13.

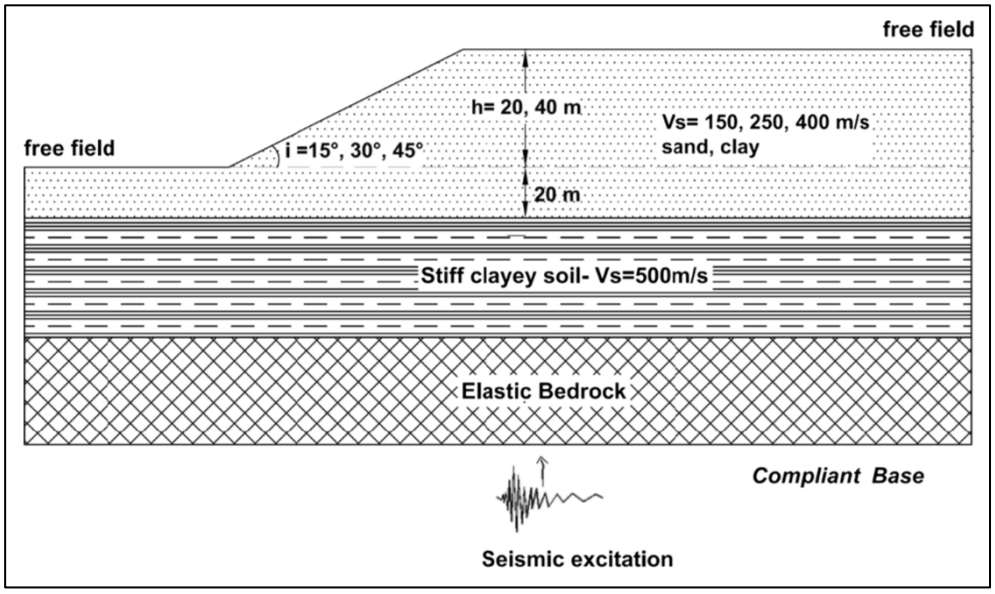

Figure 2.12 Layout of the slope geometry for Fotopoulo and Pitilakis (2015)

According to Figure 2.13, the standard deviation of a simple model of slope displacements with PGA was found to be 0.93 in Ln units. Because the objective of this study was to propose predictive relationships for seismically induced slope displacements using numerical analyses results, scalar or vector predictive models based on different ground motion IMs were tested. In the vector predictive models, reported standard deviations of the study were varied between 0.61 to 0.75 in Ln unit.

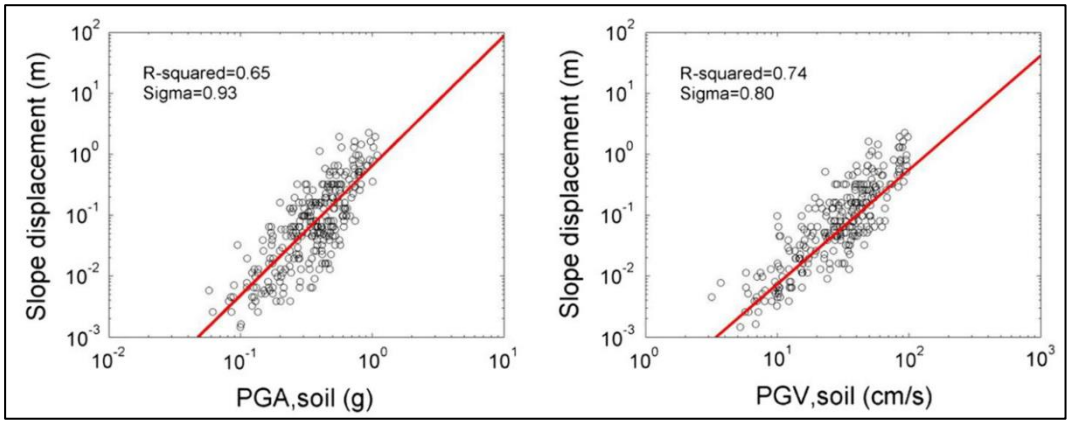

Figure 2.13 Relationship between seismic slope displacements and different IMs by Fotopoulo and Pitilakis (2015)

Athanasopoulos-Zekkos et al. (2016) provided guidelines for the ground motion selection for computation of seismic slope displacements of earthen levees. For this purpose, they analysed 3 different cross-sections (shown in the Figure 2.14) using approximately 1500 input ground motions. Ground motions were selected from PEER database using following criteria: M_w= 5.5-7.7, epicentral distances varying between 20-110 km, $V_{s,30}$>180 m/s, PGV < 100 cm/s and peak ground displacement (PGD) values smaller than 100 cm. Using scale factors varying between 0.5 and 2.0, selected ground motions were scaled up to PGA=0.4g. For each analyses case shown in Figure 2.14, the Newmark-type seismic slope displacements were calculated for different failure surfaces.

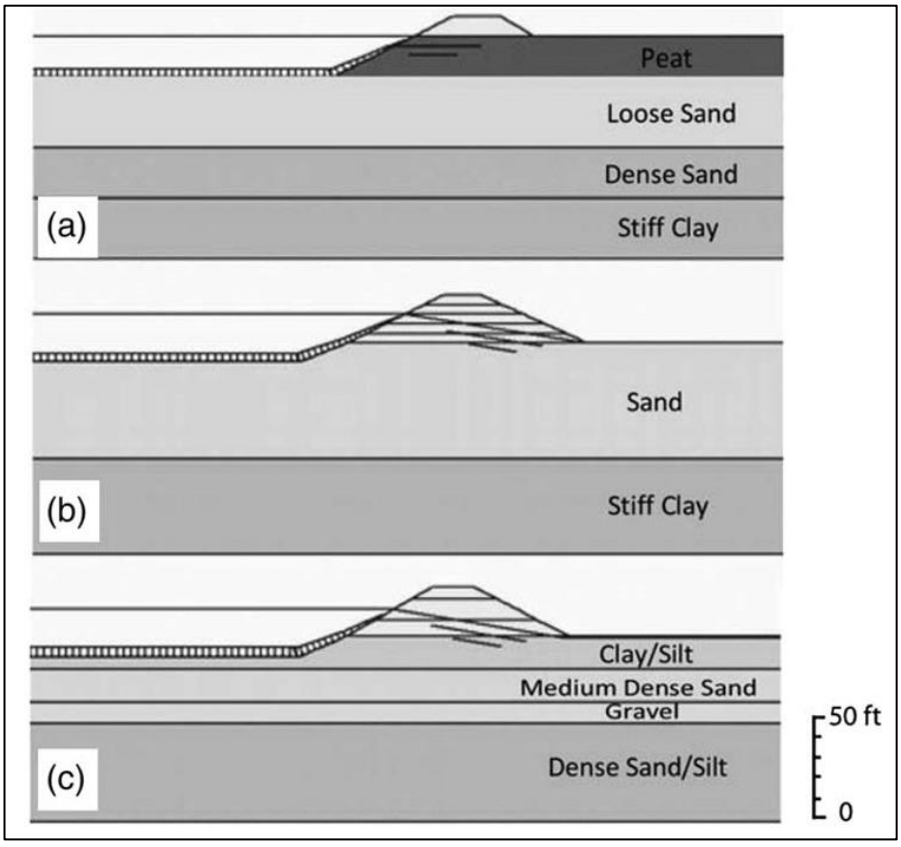

Figure 2.14 Levee geometry and soil stratigraphy used in analyses by Athanasopoulos-Zekkos et al. (2016)

In this study, various ground motion IMs were evaluated using analysis of residuals (an example is given Figure 2.15). However, a non-linear model based on PGA and PGV was proposed. Figure 2.15 shows that the residuals of the final model were biased to negative values, which was explained as a conservative result by the authors. A single value for the standard deviation was not presented in this study;

however, the scatter of calculated displacements with ground motion IMs was significant.

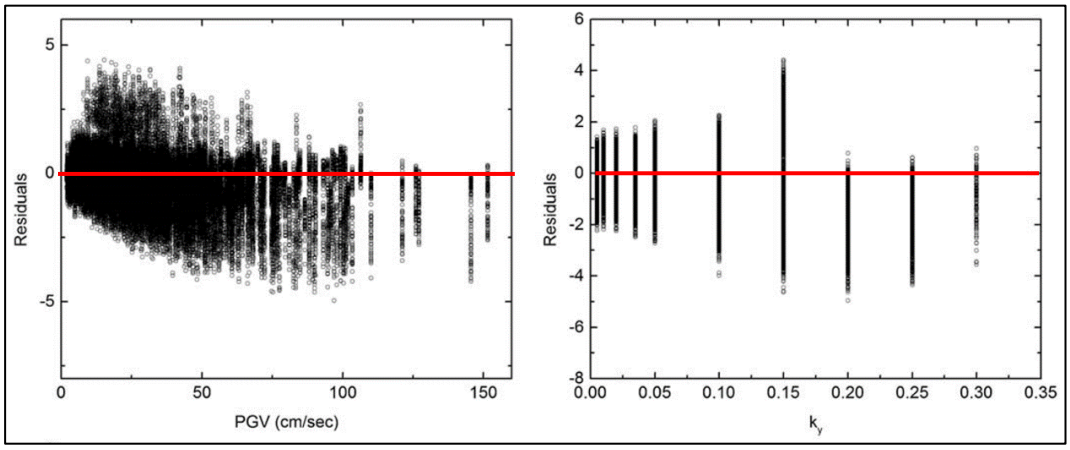

Figure 2.15 Distribution of residuals with PGV and yield coefficient by Athanasopoulos-Zekkos et al. (2016)

Peterman and Rathje (2017) aimed to examine the effects of ground motion selection technique on the rigid sliding block displacements. Different algorithms and tools were used to select the ground motions that were consistent with the target acceleration response spectrum: the two-step semi-automated algorithm developed by Kottke and Rathje (2008) was utilized to select the ground motions that fit to the uniform hazard spectrum and conditional mean spectrum for a particular site. Figure 2.16 shows that the standard deviation of the estimated slope displacements varied between 0.53 to 0.99 in Ln units, depending on the selected ground motion suite. Result of this study showed that selecting and scaling the ground motions to fit the uniform hazard spectrum is not suitable; ground motions should be selected by considering hazard compatible PGA values and conditional PGV and I_a values for sliding block analyses.

Motion suite	Median PGV (cm/s)	σ_{lnPGV}	Median Ia (m/s)	σ_{lnIa}
Target	32.0	0.53	1.9	0.93
UHS	70.4	0.67	7.1	0.68
CMS	31.5	0.39	3.8	0.46
GCIM PGV	31.8	0.29	3.6	0.97
GCIM Ia	22.9	0.71	2.0	0.95
GCIM PGV-Ia	30.1	0.81	1.9	0.99

Figure 2.16 The standard deviations calculated by Peterman and Rathje (2017)

CHAPTER 3

SELECTION OF GROUND MOTIONS, SLOPE GEOMETRIES AND GEOTECHNICAL PARAMETERS FOR NUMERICAL ANALYSIS

The primary objective of this study is to model the uncertainty in the estimated slope displacements due to the variability in the input motion selection. Selection of the candidate input ground motions is quite important and it may have a significant impact on the results. At the beginning of this chapter, the procedure followed for the selection and scaling of input ground motions are presented in details. Definition of the slope geometries and the estimation of geotechnical engineering parameters are also critical, since analysed cases are selected to cover a large range in terms of factor of safety for static case and slope angle. Different factor of safety values are created by various soil strength parameters combined with various slope angles. The efforts for developing the analysis cases are summarized in this chapter.

3.1 The Procedure for Selecting and Scaling of Input Ground Motions

The preliminary set of ground motions are gathered from the PEER Next Generation Attenuation (NGA) West 2 database, considering only one condition: the ground motions recorded on "rock" sites (the average shear wave velocity at the first 30m, V_{S30} should be at least 760 m/s, representing the B/C boundary of National Earthquake Hazards Reduction Program - NEHRP site classes) (Building Seismic Safety Council, 2004) are compiled. From this preliminary dataset, recordings from small (M_w<5) events and recordings with rupture distances (R_{RUP}) more than 100km are eliminated to prevent the need for very large scale factors in numerical analysis. In addition to that, the recordings classified as "pulse-like" are eliminated to exclude the recordings that might show near fault characteristics. Not putting any specific magnitude and distance limits for selecting the ground motions might be

contradictory with the current practice of choosing the appropriate magnitude and distance limits based on the scenario spectrum. However, Watson-Lamprey and Abrahamson (2006) showed that the average response of the non-linear system is not simply based on magnitude, distance, and spectral shape.

In order to eliminate the recordings that have significantly lower or higher spectral accelerations than the median (or expected) spectrum, candidate ground motions are divided into 12 groups based on their magnitudes and rupture distances. Each group includes the recordings from 1-magnitude unit and 25km distance bins, e.g. M5-M6, D0-D25km range as shown in Figure 3.1(a). Figure 3.1 and Figure 3.2 are used for the visual inspection of the spectra in each group: solid black lines represent the median and the broken black lines show median $\pm 1\sigma$ range for each group, and the recordings outside these ranges are eliminated from the candidate ground motion list.

Remaining ground motions are assessed by their number of recorded data points and their durations; records that have more than 25.000 data points are eliminated to decrease the computing time for dynamic numerical analyses. Additionally, ground motions that have a predominant period larger than 0.7 sec are discarded in order to avoid the possible site amplification effects of softer soil layers on the top of the soil profile of the recording station. Finally, the peak ground acceleration (PGA) values of both horizontal components of the selected recordings are compared. If there is more than 40% difference between the PGA values of the two orthogonal components, then this recordings is eliminated to avoid possible directionality effects. The final set of 50 recordings with both horizontal components (100 recordings in total) is listed in Table 3.1 with the important record properties.

Distribution of the selected recordings with magnitude, distance, V_{S30}, and fault mechanism is presented in Figure 3.3. According to Figure 3.3(a), the final dataset has 25 record pairs from magnitude 5-6 earthquakes, 20 record pairs from magnitude 6-7 earthquakes, and only 5 record pairs from magnitude 7-8 earthquakes. Figure 3.3(b) shows that the selected recordings are almost uniformly distributed with distance: there are 11 recording pairs with R_{RUP} varying between 0-25 km, 10 recording pairs with R_{RUP}=25-50 km, 15 recording pairs with R_{RUP} varying between 50-75 km, and 14 recording pairs with R_{RUP}=75-100 km.

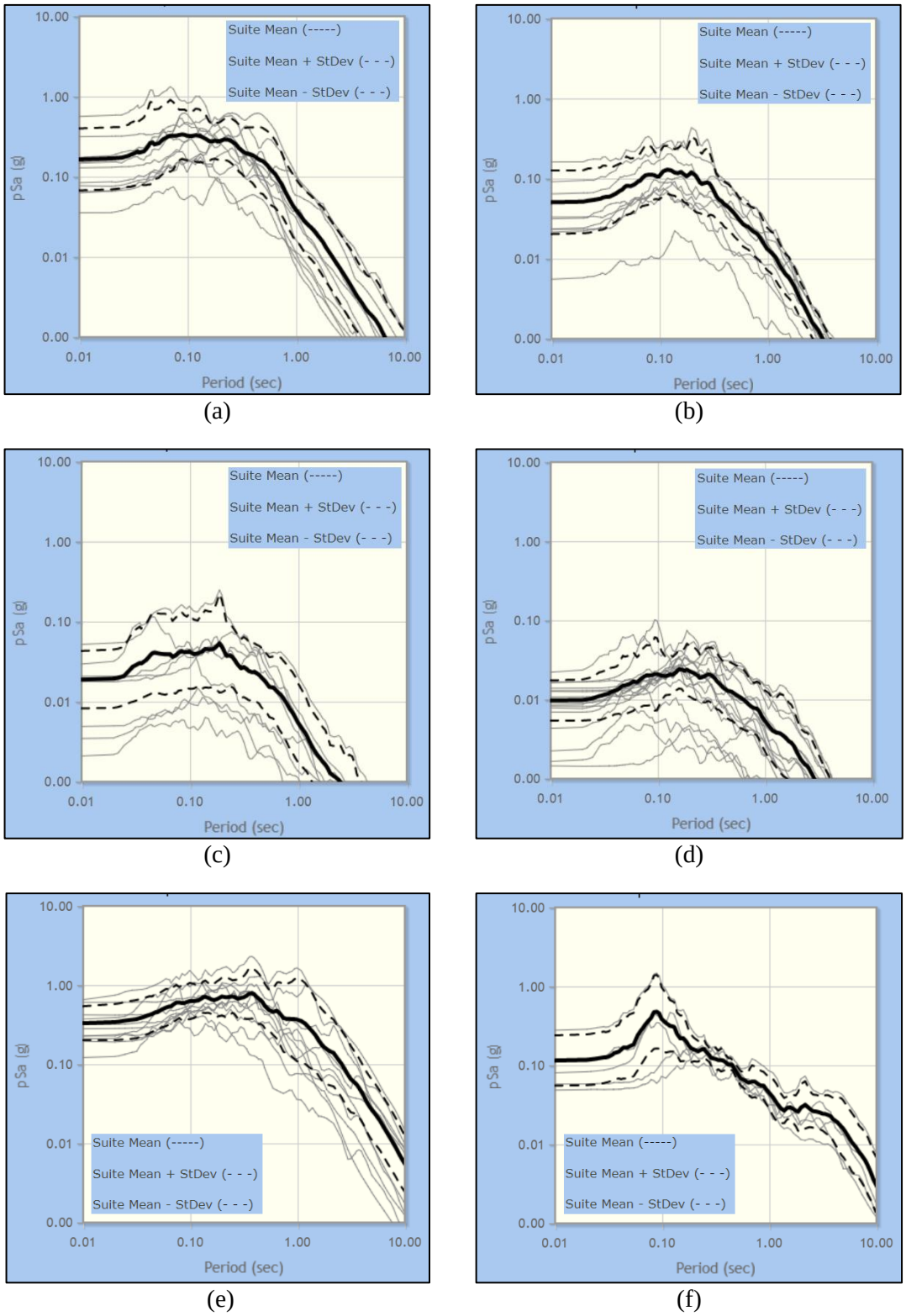

Figure 3.1 Response spectra of recordings and mean response spectrum of each bin (solid line) with ±1 standard deviation range (broken lines) for: (a) Magnitude 5-6 Distance 0-25, (b) Magnitude 5-6 Distance 25-50, (c) Magnitude 5-6 Distance 50-75, (d) Magnitude 5-6 Distance 75-100, (e) Magnitude 6-7 Distance 0-25, (f) Magnitude 6-7 Distance 25-50

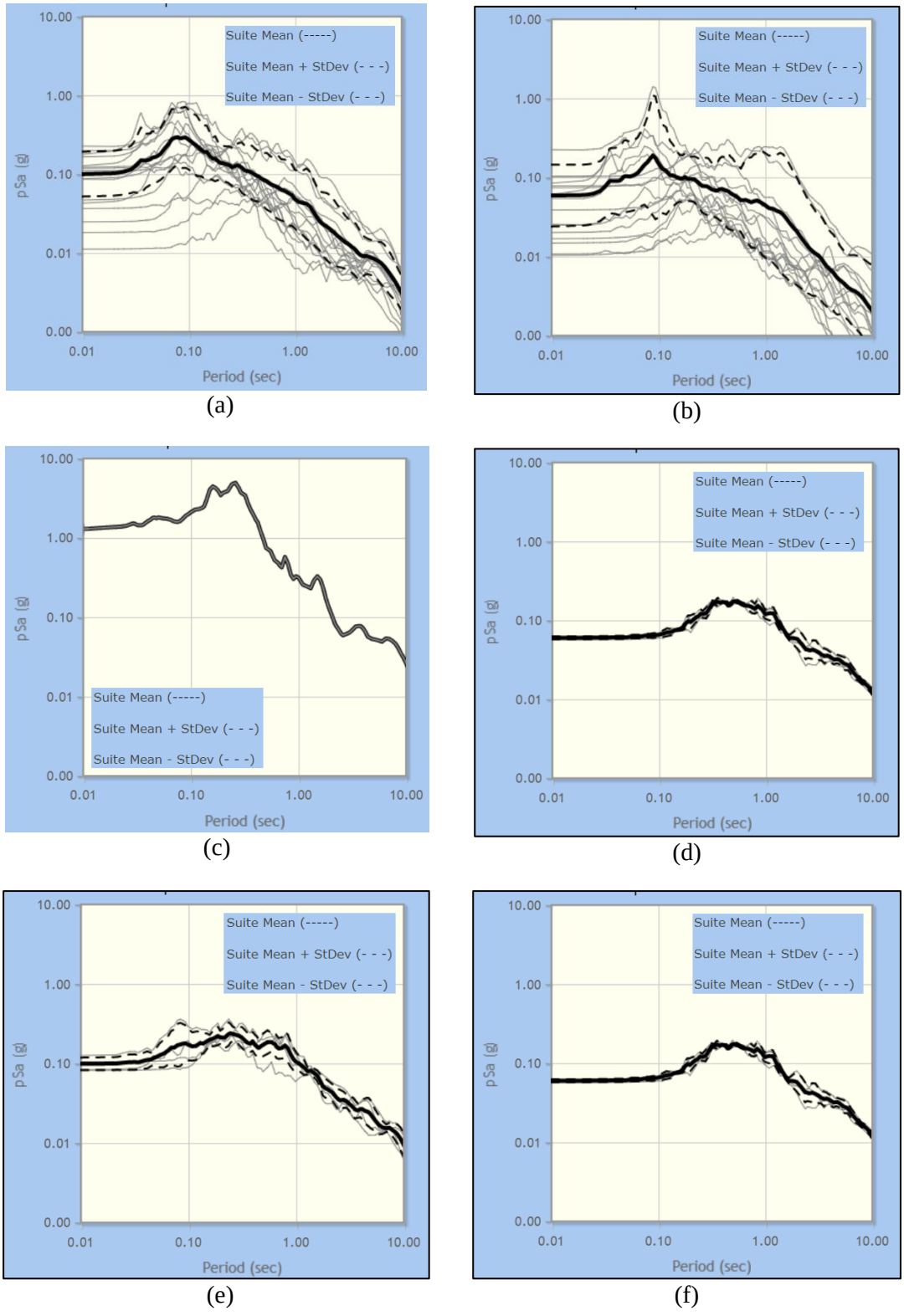

Figure 3.2 Response spectra of recordings and mean response spectrum of each bin (solid line) with ±1 standard deviation range (broken lines) for: (a) Magnitude 6-7 Distance 50-75, (b) Magnitude 6-7 Distance 75-100, (c) Magnitude 7-8 Distance 0-25, (d) Magnitude 7-8 Distance 25-50, (e) Magnitude 7-8 Distance 50-75, (f) Magnitude 7-8 Distance 75-100

Table 3.1 The ground motion pairs selected for the dynamic numerical analysis and the properties of the selected recordings

PEER Record Sequence Number	Earthquake Name	Magnitude (M_w)	Mechanism	R_{jb} (km)	R_{rup} (km)	V_s^{30} (m/sec)	Lowest Useable Frequency (Hz)	Component 1 a_{max} (g)	Component 1 Predominant Period (sec)	Component 2 a_{max} (g)	Component 2 Predominant Period (sec)
23	San Francisco	5.28	Reverse	9.74	11.02	874.72	0.875	0.08577	0.14	0.09532	0.22
59	San Fernando	6.61	Reverse	89.37	89.72	813.48	0.375	0.01963	0.16	0.01526	0.14
98	Hollister-03	5.14	strike slip	9.99	10.46	1428.14	1.625	0.10025	0.1	0.14052	0.1
146	Coyote Lake	5.74	strike slip	10.21	10.67	1428.14	0.15	0.09407	0.1	0.11663	0.08
643	Whittier Narrows-01	5.99	Reverse Oblique	23.4	27.64	1222.52	0.6	0.04142	0.08	0.04861	0.12
680	Whittier Narrows-01	5.99	Reverse Oblique	6.78	18.12	969.07	0.4125	0.11177	0.36	0.09478	0.34
703	Whittier Narrows-01	5.99	Reverse Oblique	47.25	50.39	996.43	1	0.06196	0.16	0.06585	0.12
788	Loma Prieta	6.93	Reverse Oblique	72.9	73	895.36	0.125	0.08378	0.36	0.07163	0.4
789	Loma Prieta	6.93	Reverse Oblique	83.37	83.45	1315.92	0.075	0.07174	0.28	0.07355	0.46
797	Loma Prieta	6.93	Reverse Oblique	74.04	74.14	873.1	0.125	0.07889	0.12	0.09289	0.54
1011	Northridge-01	6.69	Reverse	15.11	20.29	1222.52	0.175	0.10329	0.12	0.15899	0.24
1091	Northridge-01	6.69	Reverse	23.1	23.64	996.43	0.25	0.15101	0.38	0.13907	0.2
1347	Chi-Chi_ Taiwan	7.62	Reverse Oblique	57.69	61.06	996.51	0.025	0.09461	0.08	0.08236	0.24
1442	Chi-Chi_ Taiwan	7.62	Reverse Oblique	95.31	97.39	807.68	0.025	0.03716	0.38	0.0432	0.36
1452	Chi-Chi_ Taiwan	7.62	Reverse Oblique	92.01	94.16	887.68	0.025	0.03676	0.54	0.0505	0.34
1518	Chi-Chi_ Taiwan	7.62	Reverse Oblique	55.14	58.09	999.66	0	0.06344	0.56	0.05337	0.1
1649	Sierra Madre	5.61	Reverse	37.63	39.81	996.43	0.8	0.09793	0.22	0.12529	0.2
1715	Northridge-06	5.28	Reverse	13.15	17.14	1222.52	1.5	0.05461	0.24	0.05255	0.26
2207	Chi-Chi_ Taiwan-02	5.9	Reverse	78.6	79.68	804.36	0.375	0.00964	0.12	0.01295	0.08
2215	Chi-Chi_ Taiwan-02	5.9	Reverse	56.46	58.8	789.18	0.375	0.01451	0.24	0.01485	0.24
2296	Chi-Chi_ Taiwan-02	5.9	Reverse	80.14	80.4	996.51	0.25	0.01264	0.34	0.01078	0.2
2396	Chi-Chi_ Taiwan-02	5.9	Reverse	78.11	78.38	999.66	0.375	0.01032	0.34	0.00928	0.48
2753	Chi-Chi_ Taiwan-04	6.2	strike slip	39.3	39.32	804.36	0.05	0.05339	0.08	0.05899	0.1
2989	Chi-Chi_ Taiwan-05	6.2	Reverse	69.76	74.16	804.36	0.06	0.05736	0.1	0.06431	0.1
2995	Chi-Chi_ Taiwan-05	6.2	Reverse	44.36	45.03	789.18	0.075	0.03207	0.24	0.03635	0.32

Table 3.1 The ground motion pairs selected for the dynamic numerical analysis and the properties of the selected recordings (continued)

PEER Record Sequence Number	Earthquake Name	Magnitude (M_w)	Mechanism	R_{jb} (km)	R_{rup} (km)	V_s^{30} (m/sec)	Lowest Useable Frequency (Hz)	Component 1 a_{max} (g)	Component 1 Predominant Period (sec)	Component 2 a_{max} (g)	Component 2 Predominant Period (sec)
3318	Chi-Chi_ Taiwan-06	6.3	Reverse	62.46	63.26	804.36	0.05	0.03438	0.08	0.03159	0.08
3542	Chi-Chi_ Taiwan-06	6.3	Reverse	84.03	86.38	845.34	0.125	0.02693	0.24	0.02798	0.42
3718	Whittier Narrows-02	5.27	Reverse Oblique	25.04	28.42	1222.52	1.125	0.01653	0.1	0.01652	0.12
3895	Tottori_ Japan	6.61	strike slip	99.64	99.64	760.54	0.0625	0.03974	0.08	0.03531	0.06
4083	Parkfield-02_ CA	6	strike slip	4.66	5.29	906.96	0.1875	0.2453	0.26	0.19609	0.46
4312	Umbria-03_ Italy	5.6	Normal	14.67	15.72	922	0.2875	0.0501	0.18	0.06745	0.24
4438	Molise-02_ Italy	5.7	strike slip	49.6	51.32	865	1.25	0.03875	0.18	0.03412	0.2
5483	Iwate_ Japan	6.9	Reverse	37.45	39.41	829.46	0.0375	0.08503	0.12	0.06646	0.12
5618	Iwate_ Japan	6.9	Reverse	16.26	16.27	825.83	0.025	0.22554	0.36	0.28864	0.14
5649	Iwate_ Japan	6.9	Reverse	72.44	72.44	1269.78	0.0125	0.06032	0.08	0.05993	0.08
5650	Iwate_ Japan	6.9	Reverse	64.27	64.27	891.55	0.0125	0.13496	0.14	0.14029	0.08
5655	Iwate_ Japan	6.9	Reverse	68.03	68.03	922.89	0.025	0.11885	0.08	0.10745	0.1
5679	Iwate_ Japan	6.9	Reverse	56.72	56.72	933.96	0.025	0.0819	0.06	0.09306	0.08
8165	Duzce_ Turkey	7.14	strike slip	4.21	4.21	760	0.0375	1.03058	0.26	0.75063	0.26
8167	San Simeon_ CA	6.52	Reverse	37.92	37.97	1100	0.0375	0.03439	0.24	0.0465	0.2
8707	40204628	5.45	strike slip	30.45	30.75	760	0.3625	0.02617	0.1	0.01971	0.12
8715	40204628	5.45	strike slip	85.93	86.03	760	0.925	0.00538	0.18	0.00603	0.3
8728	40204628	5.45	strike slip	88.26	88.36	760	0.2125	0.0049	0.16	0.00476	0.2
8819	14383980	5.39	Reverse Oblique	38.48	41.17	760	0.3	0.01971	0.12	0.02337	0.16
8845	14383980	5.39	Reverse Oblique	80.94	82.63	1131	0.3	0.00542	0.14	0.00712	0.16
8877	14383980	5.39	Reverse Oblique	57.15	58.48	1043	0.1875	0.0109	0.14	0.01391	0.16
8986	14151344	5.2	strike slip	73.57	75.27	796	0.25	0.0109	0.14	0.01439	0.18
9014	14151344	5.2	strike slip	74.08	75.24	805	0.2625	0.0169	0.06	0.02346	0.04
9050	14151344	5.2	strike slip	91.03	92.41	1188	0.225	0.00418	0.16	0.00646	0.16
20130	40204628	5.45	strike slip	92.7	92.8	760	0.1908422	0.00852	0.28	0.00916	0.22

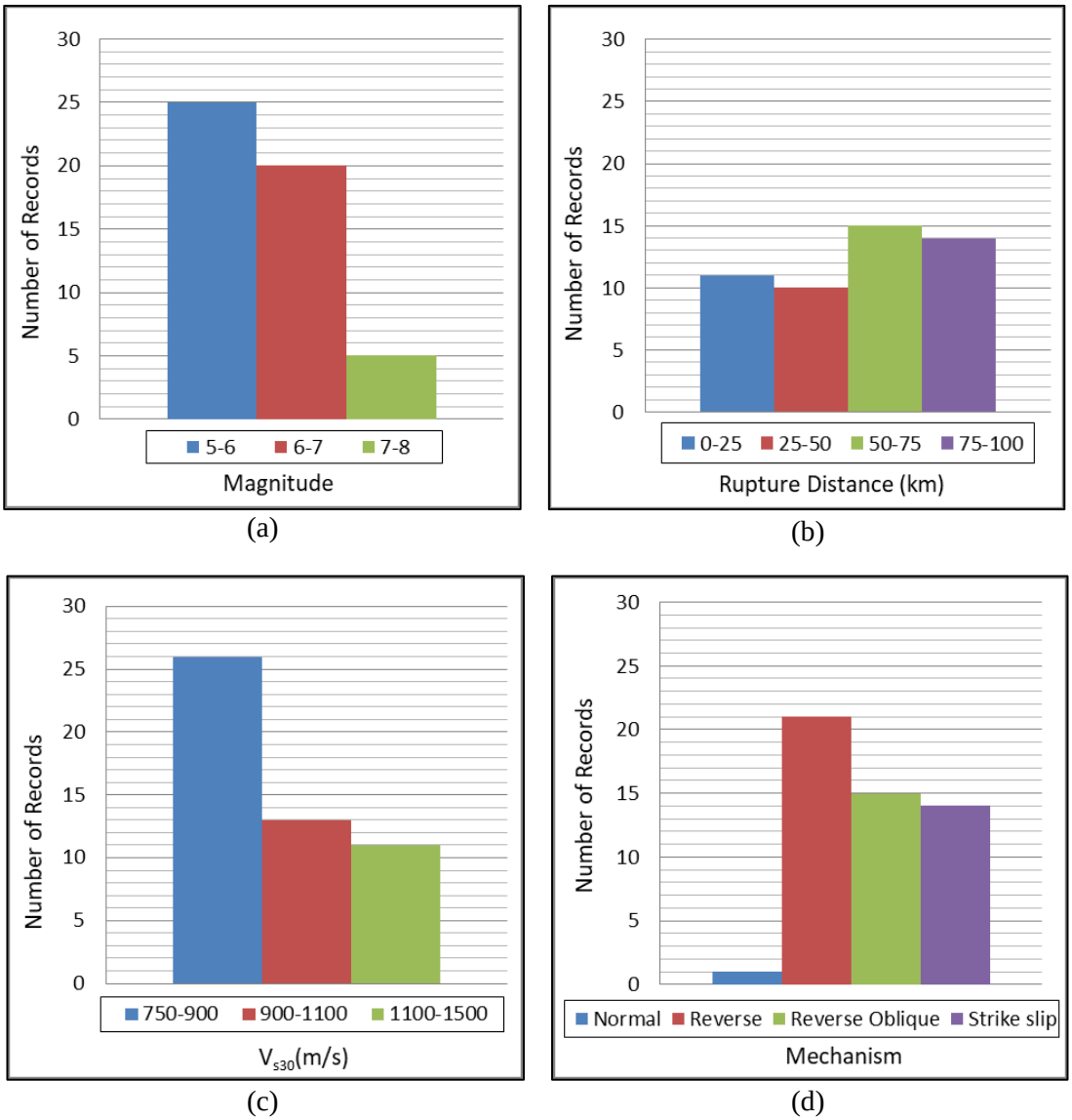

Figure 3.3 Distribution of the selected recordings with (a) magnitude, (b) rupture distance, (c) V_{S30}, and (d) fault mechanism

Figure 3.3(c) shows that the V_{s30} values of the recording stations for the selected ground motions go up to 1500 m/sec. There are 26 recording pairs between V_{s30}=750-900 m/sec, 13 recording pairs between V_{s30}=900-1100 m/sec and 11 recording pairs between V_{s30}=1100-1500 m/sec. The distribution of the recordings with respect to fault mechanism is not uniform. There is only one record pair from normal earthquakes because the number of recordings from normal earthquakes is very limited in the PEER database. According to Figure 3.3(d), only 1 record pair from normal fault mechanism, 21 record pairs from reverse fault mechanism, 15 record pairs from reverse-oblique fault mechanism, and 14 record pairs from strike-slip fault mechanism are selected.

The PGA values of the selected recordings reach up to 0.29g, except for one recording from Düzce Earthquake (RSN#8165) with PGA=1.0g. To cover a larger range of ground shaking levels, selected 100 recordings are scaled with the scale factors of 2.5 and 5 for PGA. As a result, the final dataset of 300 recordings are obtained and the maximum PGA value of the recordings in the final dataset is equal to 1.0g.

3.2 Slope Geometries and Geotechnical Parameters: Static Slope Stability Analysis

Various factors such as slope geometry, soil profile, material properties and groundwater conditions affect the permanent slope displacement in addition to the input ground motions. Akbaş et al. (2018) used the results of pseudo- static slope stability analysis to develop a simple seismic demand model for pseudo-static factor of safety. In that study, several parameters related to the soil's effective shear strength and slope geometry were evaluated where the factor of safety in static condition was chosen as the single parameter to represent the combination of geotechnical factors.

In this study, slope angle was also added to the simplified seismic demand model since its effect on the calculated factor of safety (both in static and pseudo-static conditions) was very significant. Based on the previous findings, the factor of safety in static condition and the slope angle are selected as the critical parameters that mainly influence the results.

Eight different cases having a slope height equal to 10 m are studied in the numerical analysis with various slope angle and effective shear strength parameters of soil. The slope geometry for the first four cases (Cases 1a, 1b, 1c and 1d), which is named Set 1, is the same as shown in Figure 3.4: the slope angle is kept constant at 28˚, while factor of safety in static condition is varied between 1.2 and 2.3. For the other four cases (Cases 2a, 2b, 2c 2d and 2e), which is named Set 2, the slope angle is varied between 20˚ and 41˚, while the static factor of safety is kept constant at FS=1.5. The simplified sketch of last four cases is shown in Figure 3.5.

After the geometrical properties of the slope (i.e., slope height and inclination) are determined, required static factor of safety is maintained by selecting appropriate effective material properties (i.e., values for cohesion and internal friction angle). The effective soil parameters used for each case are provided in Table 3.2. Unit weight of the soil is selected as 20 kN/m^3 for each case.

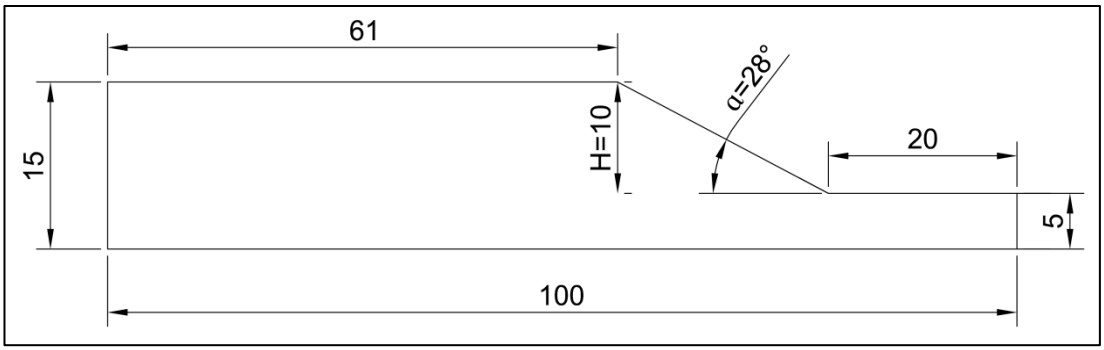

Figure 3.4 Geometry of Set 1 cases with variable factor of safety and constant slope angle (all dimensions are in meters)

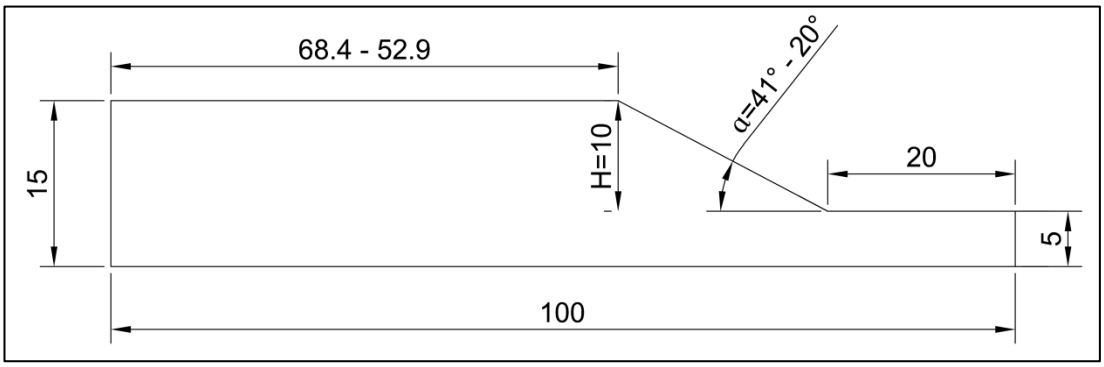

Figure 3.5 Geometry of Set 2 cases with constant static factor of safety and variable slope angle (all dimensions are in meters)

Table 3.2 The effective soil parameters utilized for the safety analyses for static condition

Set 1 cases (α = 28º)				Set 2 cases (FS = 1.5)			
Case Id	FS	c (kPa)	ϕ (°)	Case Id	Slope Angle (º)	c (kPa)	ϕ (°)
1a	1.2	1	30	2a	20	5	22
1b	1.5	5	30	2b	24	5	26
1c	1.7	5	35	2c	28	5	30
1d	2.3	5	44	2d	34	5	37
				2e	41	5	44

The static factor of safety values for analysed cases are calculated using the strength reduction (c/phi reduction) method in PLAXIS 2D software. Although the resultant

displacement amounts are not relevant in strength reduction method, potential failure planes for each case are identified by evaluating the incremental total displacement contours at the end of static analysis as shown in Figure 3.6 to Figure 3.13.

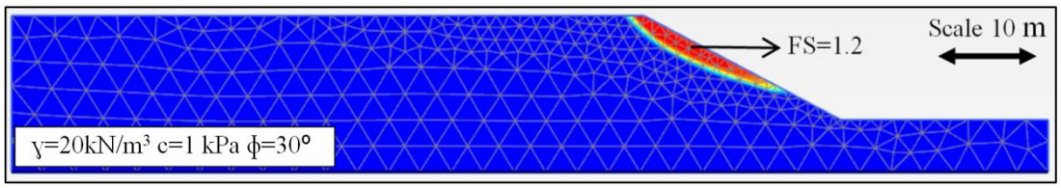

Figure 3.6 Failure surface for the static analysis of Case Id 1a

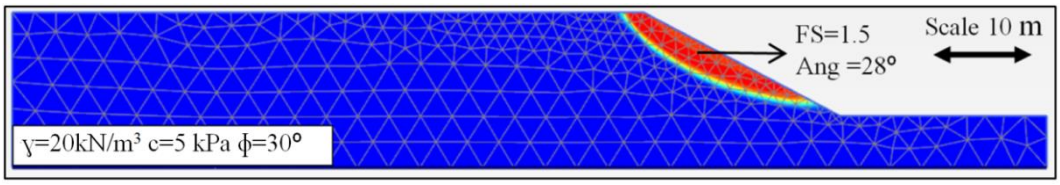

Figure 3.7 Failure surface for the static analysis of Case Id 1b/2c

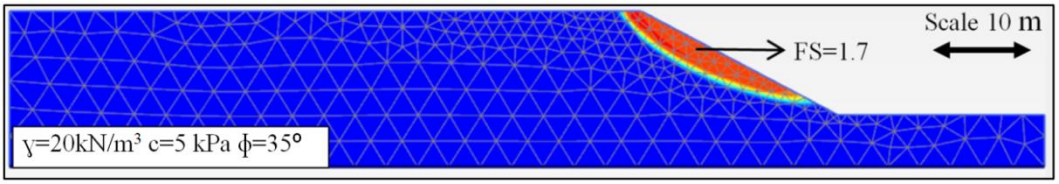

Figure 3.8 Failure surface for the static analysis of Case Id 1c

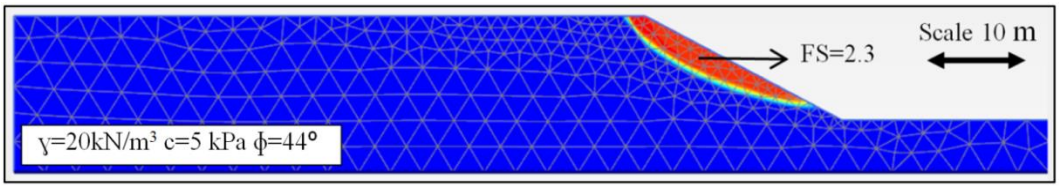

Figure 3.9 Failure surface for the static analysis of Case Id 1d

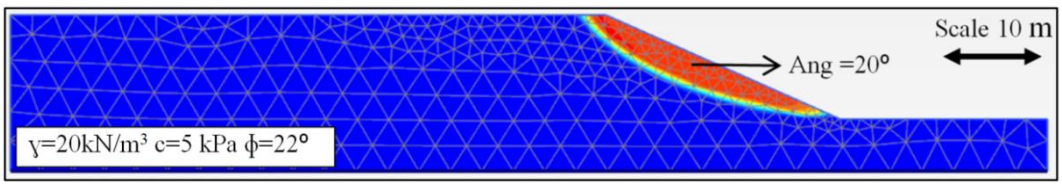

Figure 3.10 Failure surface for the static analysis of Case Id 2a

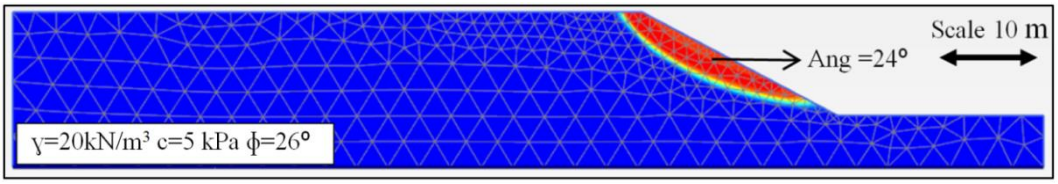

Figure 3.11 Failure surface for the static analysis of Case Id 2b

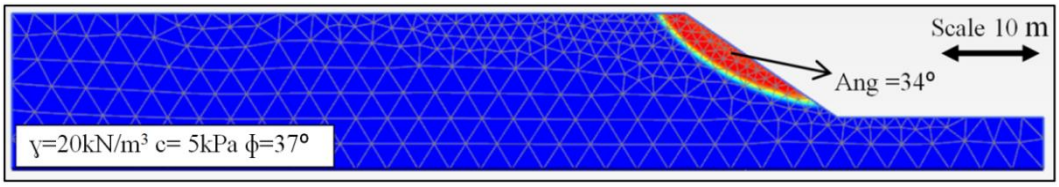

Figure 3.12 Failure surface for the static analysis of Case Id 2d

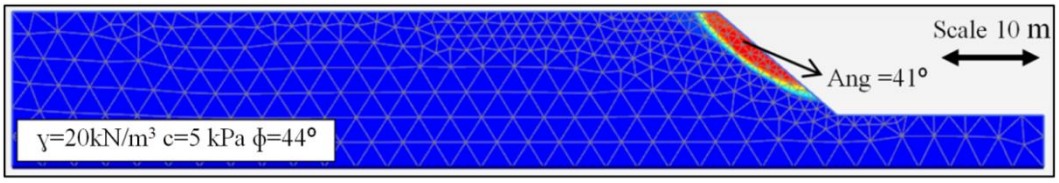

Figure 3.13 Failure surface for the static analysis of Case Id 2e

3.3 Boundary Conditions and Geotechnical Parameters for Dynamic Analysis

In order to define the geotechnical parameters required for the dynamic analysis, a representative soil model is assigned to each profile. For the cohesionless granular soils (Case 1a, 1b, 1c, 1d, 2c, 2d and 2e) the representative average Standard Penetration Test blow counts (SPT - $(N_1)_{60}$ values – overburden and energy corrected) are determined based on the correlation between SPT - $(N_1)_{60}$ and internal friction angle that was proposed by Stroud (1988) for sands (Figure 3.14). Deformation modulus of soil, E_s, values are estimated based on the representative SPT - $(N_1)_{60}$ values using the FHWA (2002a) recommendations given in Table 3.3. In order the represent the average behaviour of the cohesionless soils, E_s values are calculated as $E_s \cong 850(N_1)_{60}$.

Table 3.3 SPT - $(N_1)_{60}$ vs. E_s correlations (FHWA, 2002a)

Soil Type	E_s (kPa)
Silts, Sandy Silts, Slightly Cohesive Mixtures	400 $(N_1)_{60}$
Clean Fine to Medium Sands and Slightly Silty Sands	700 $(N_1)_{60}$
Coarse Sands and With Little Gravel	1000 $(N_1)_{60}$
Sandy Gravels	1200 $(N_1)_{60}$

For the cohesive soil profiles (Cases 2a and 2b), the plasticity index (PI) values are required to select suitable modulus degradation curves. For that purpose, the correlation between PI and the internal friction angle suggested by Terzaghi, Peck and Mesri (1996) (Figure 3.15) and by Das (1985) (Figure 3.16) are utilized. Based on these correlations, PI values are estimated as 80% and 40% for Case #2a and Case #2b, respectively. The correlation given by Stroud (1988) in Figure 3.17 is used to determine the E_s values for Cases #2a and #2b, assuming $E_s/N_{60} = 0.67$.

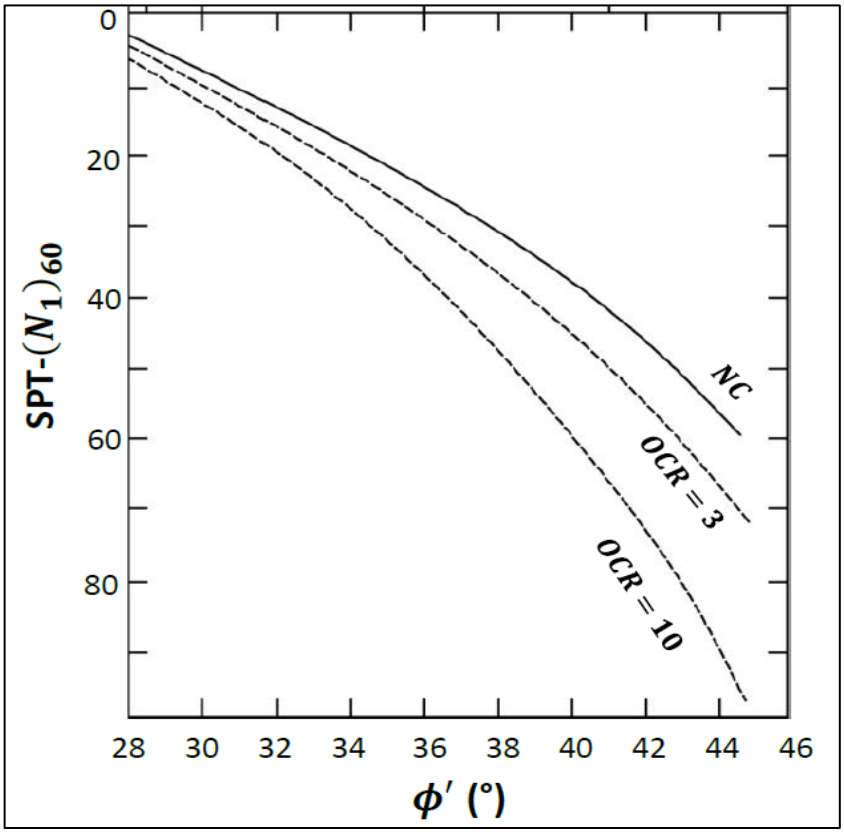

Figure 3.14 SPT - $(N_1)_{60}$ - ϕ correlation for sands (Stroud, 1988)

In order to define the maximum shear modulus (G_{max}) and shear strain corresponding to 70% of G_{max} ($\gamma_{0.7}$), the average shear wave velocity value should be estimated for each case. Imai et al. (1976) suggested a relationship between the shear wave velocity (V_s) and uncorrected SPT-N value for various soil types as shown in Table 3.4.

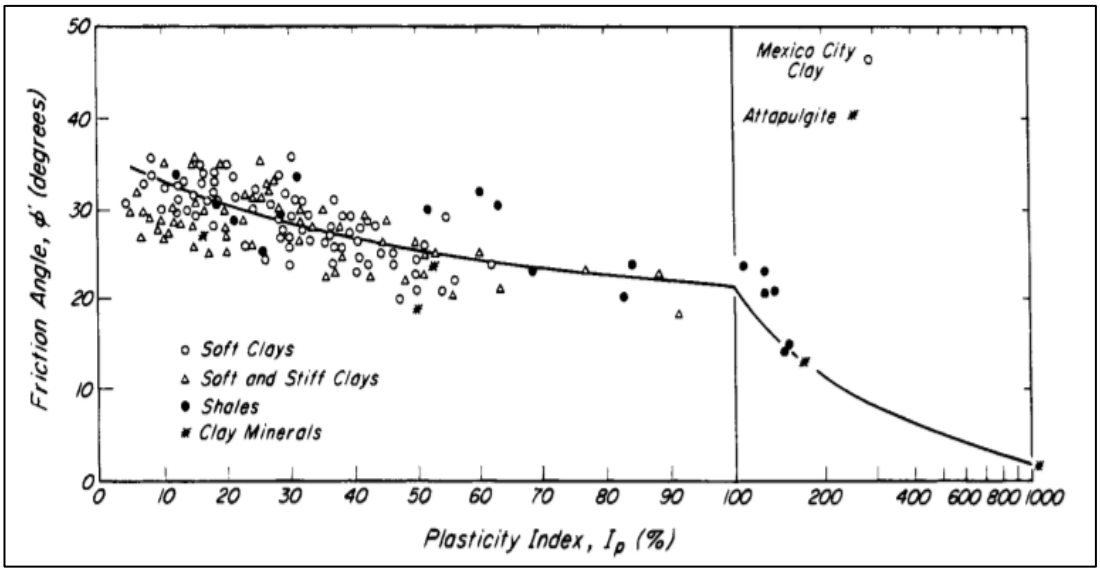

Figure 3.15 Correlation between plasticity index and effective friction angle (by Terzaghi, Peck and Mesri, 1996)

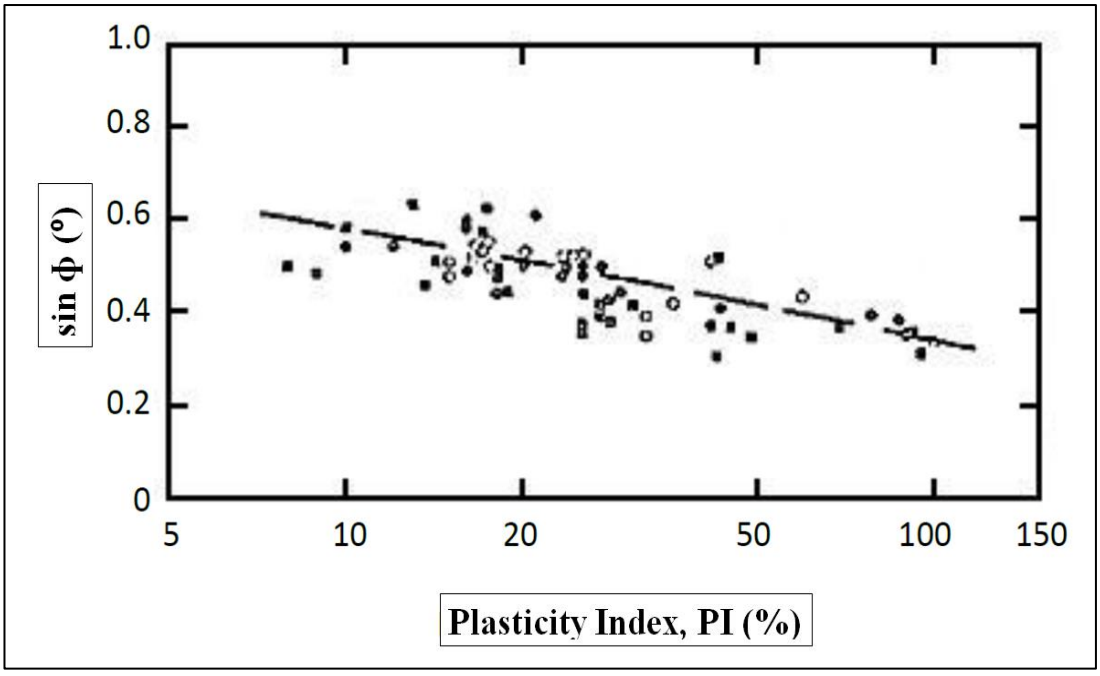

Figure 3.16 Plasticity index versus effective friction angle (by Das, 1985, taken from Erol and Çekinmez, 2014)

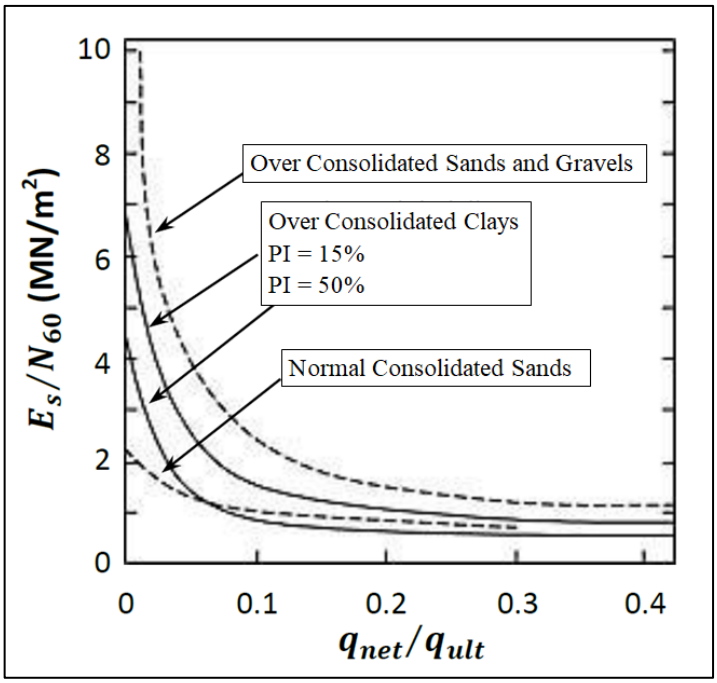

Figure 3.17 E_s - SPT-N correlation used for clay-like profiles (by Stroud, 1988, taken from Erol and Çekinmez, 2014)

The representative SPT - $(N_1)_{60}$ value assigned to each profile is uncorrected to SPT-N using Equation 15. The average and clayey alluvium relationships are used to calculate V_s form SPT-N for sand-like and clay-like profiles. After the V_s value is estimated, G_{max} is calculated for each case using Equation 16. The shear strain corresponding to 70% of G_{max} ($\gamma_{0.7}$) is estimated from the modulus degradation curves proposed by Vucetic and Dobry (1991) as shown in Figure 3.18. For sand-like profiles, PI=0 curve is used, while the representative PI values estimated for Cases #2a and #2b are utilized for clay-like profiles.

$$(N_1)_{60} = \left(9.78 * \sqrt{\frac{1}{\sigma'_{v,0}}}\right) * N_{60} \qquad \text{(Eq.15)}$$

$$Gmax = p \times Vs^2 \qquad \text{(Eq. 16)}$$

Table 3.4 Relation between shear wave velocity and SPT resistance (by Imai et al., 1976)

Type of Soil	V_s (m/s)
Sandy Alluvium	$102.0\ N^{0.29}$
Clayey Alluvium	$80.6\ N^{0.33}$
Average Value	$89.8\ N^{0.34}$

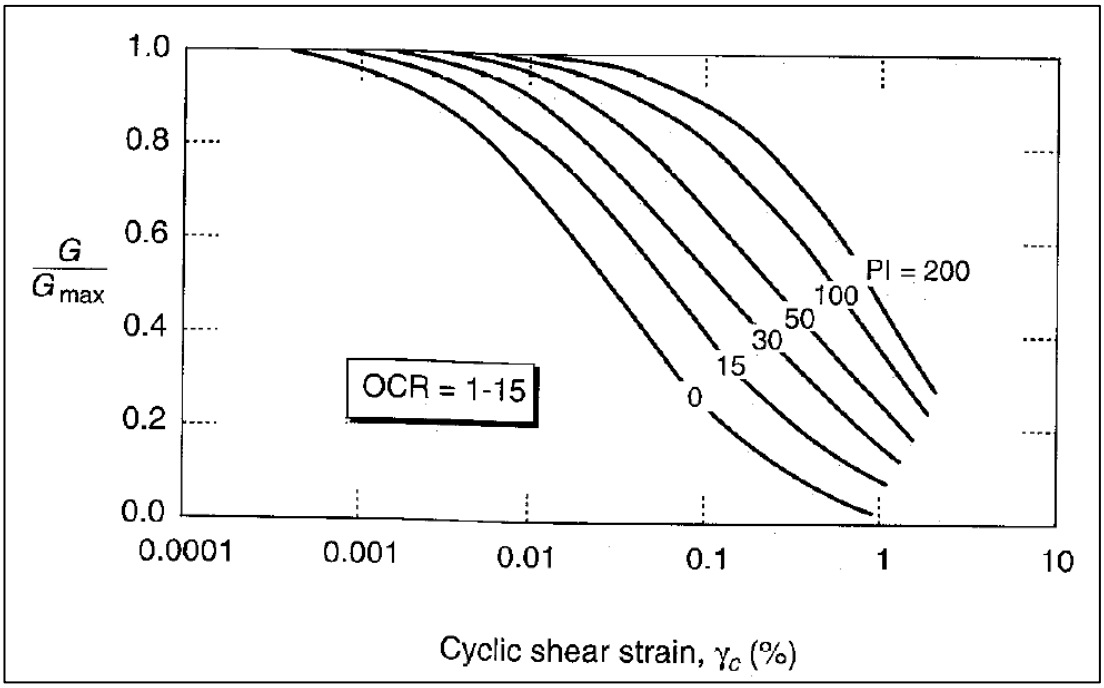

Figure 3.18 Modulus degradation curves for fine-grained soils of different plasticity (by Vucetic and Dobry, 1991)

All geotechnical engineering parameters necessary for dynamic numerical analysis are summarized in Table 3.5. In the analysis, the water table is assumed very deep; therefore, groundwater effects are neglected and soils are dry and drained condition.

Table 3.5 Geotechnical engineering parameters used in the dynamic numerical analysis

Slope Angle = 28º						FS = 1.5					
Case #	E (kPa)	V_s (m/s)	G_{max} (kPa)	PI (%)	$\gamma_{0.7}$ (%)	Case #	E (kPa)	V_s (m/s)	G_{max} (kPa)	PI (%)	$\gamma_{0.7}$ (%)
1a	6000	170	58000	0	0.01	2a	3000	120	29000	80	0.1
1b	6000	170	58000	0	0.01	2b	4000	140	40000	40	0.08
1c	18000	250	125000	0	0.01	2c	6000	170	58000	0	0.01
1d	44000	350	245000	0	0.01	2d	25000	280	157000	0	0.01
						2e	44000	350	245000	0	0.01

The sample of the mesh used in the dynamic analysis is presented in Figure 3.19. A finer mesh size is preferred where the movement of the soil may occur and the mesh size is enlarged towards the edges of the model in order to optimize the run time. Boundaries at both sides are extended to eliminate the possible boundary effects, considering the runtime: length of the model is optimized as 100m during the test runs. As explained in the previous chapter, free field absorbing boundaries are preferred at the sides of the model to prevent spurious reflections of outward

propagating waves from artificial boundaries, while the boundary type “none” is used for the bottom edge of the model (i.e. rigid bedrock). Input ground motions are applied as acceleration time histories at the bottom edge of the model. The Rayleigh damping value is set to 1% to account for the energy dissipation during the elastic part of the cyclic response and the frequency range of the Rayleigh damping is defined as 1.8-26 Hz based on the natural frequencies of all analysis cases, also covering the predominant frequency of all input motions (Rathje and Bray, 2001).

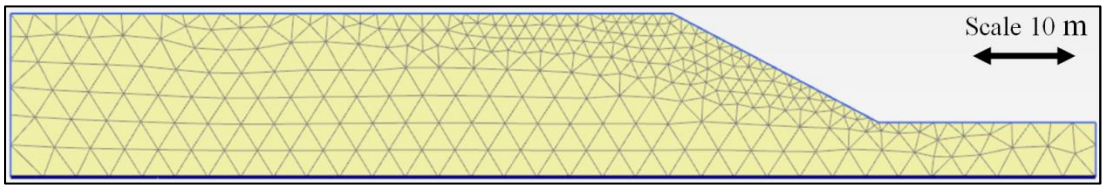

Figure 3.19 Sample of the mesh used in the dynamic analysis

The time histories of slope displacements are recorded at the centre of gravity of the sliding mass, in both vertical and horizontal directions. Assuming that the centre of gravity for the sliding mass might be slightly different for each dynamic analysis performed with different input ground motions, the centre of gravity of the sliding surface determined during the static analysis is selected for each analysis case for recording the displacement time histories. Figure 3.20 compares the static failure surface and the centre of gravity of the sliding mass determined in the static analysis with the contours of earthquake-induced slope displacements in dynamic analysis (Case 1b/2c, input motion RSN#4083_270 scaled by 2.5). Contours of earthquake-induced slope displacements indicates a slightly larger failure surface for dynamic case, however, the point selected for recording the time histories still (approximately) represents the centre of gravity for the sliding surface. Figure 3.21 shows an example time history for slope displacement at the centre of gravity of the sliding mass. For each dynamic analysis, the maximum and final (or permanent) slope displacement values are recorded in both horizontal and vertical directions and the resultant displacement values are calculated. In this particular example, the maximum displacement is found as 15.43cm and final displacement is equal to 14.42cm.

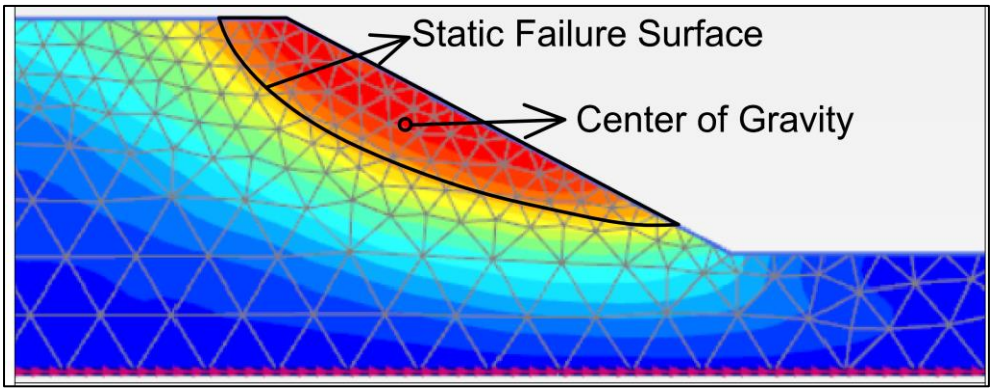

Figure 3.20 Static failure surface and the centre of gravity of the sliding mass with the contours of an earthquake induced slope displacement

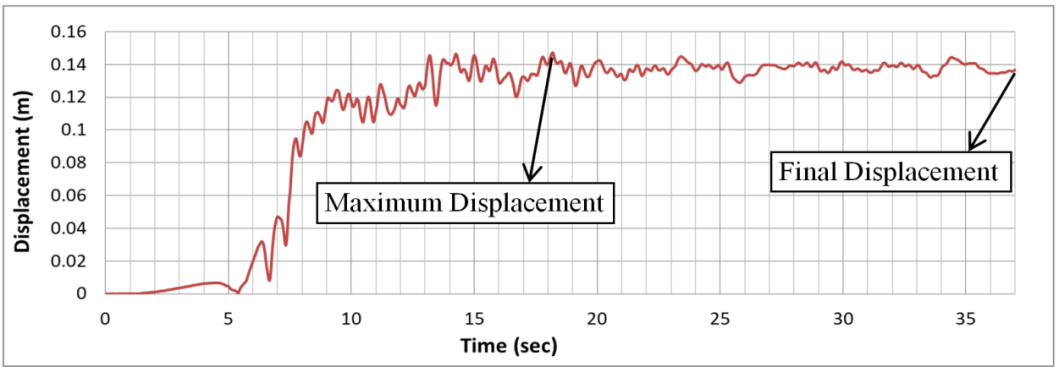

Figure 3.21 Example of displacement and time graph of centre of gravity

Figure 3.22 shows the contours of earthquake-induced slope displacement for an example dynamic analysis (Case #2a). The time history of the displacements, acceleration time history, and response spectrum are recorded at the bedrock level (Point C), at the toe (Point A) and at the centre of gravity (Point B). These outputs are compared in Figure 3.23 and Figure 3.24 for high (PGA=0.61g) and low (PGA=0.09g) ground shaking levels, respectively. Figure 3.23(a) and Figure 3.24(a) show that the slope displacements at the toe and at the centre of gravity are quite close to each other, both for high and low ground-shaking levels. The ratio of the final displacement values at Point C (bedrock) to Point B is less than 1% for the majority of the analyses. Therefore, the final displacement measurements that are directly obtained from Point B are utilized without calculating the residual (Point B-Point C) final displacement. The time of maximum displacement at Point C may be close to the time of maximum displacement at the toe or at the centre of gravity, depending on the input motion. Input ground motions are amplified significantly in

low ground shaking levels and the response spectra at the toe and at the centre of gravity are quite close to each other (Figure 3.24(c)). For higher ground shaking levels, site amplifications (and de-amplifications) are significant at short periods, but the response spectra at the toe and at the centre of gravity are different from each other (Figure 3.23(c)).

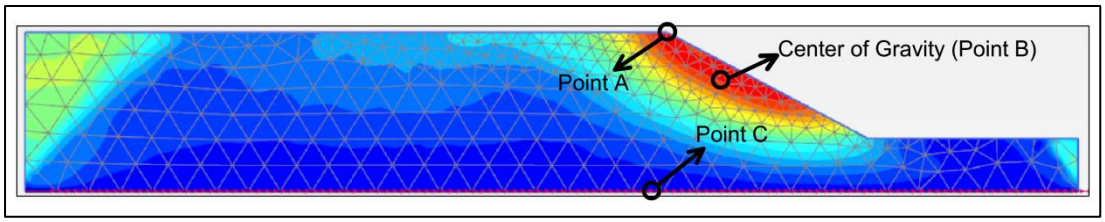

Figure 3.22 Selected data points

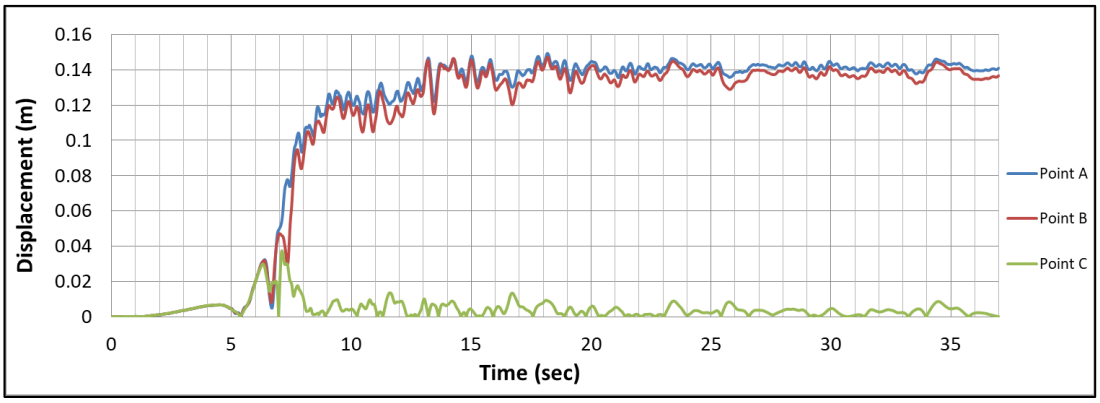

(a)

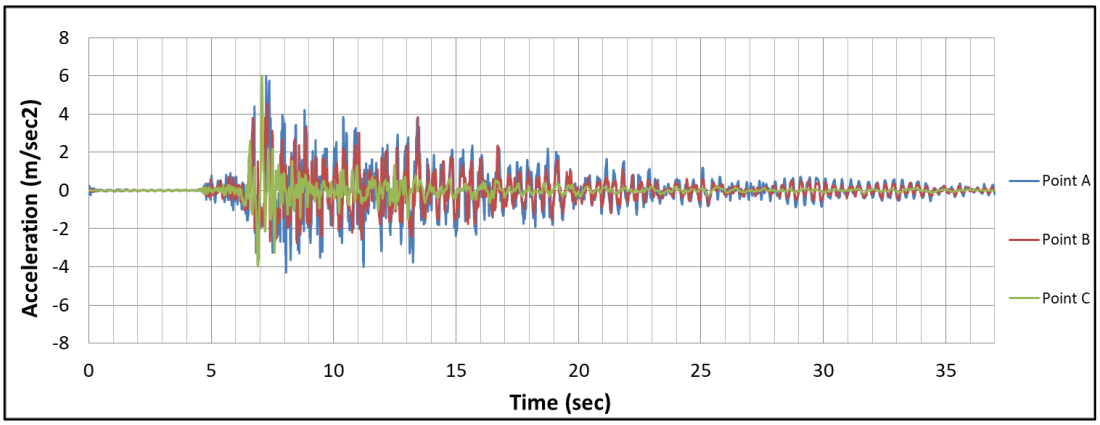

(b)

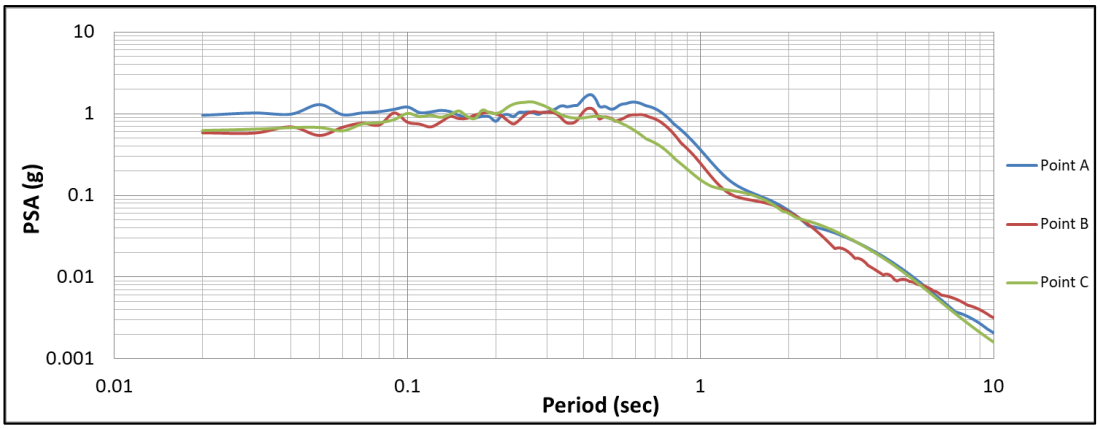

(c)

Figure 3.23 Results graphs of Case # 1b/2c soil model, analysed with RSN# 4083_270 ground motion which scaled by 2.5 (a) Displacement and Time graph, (b) Acceleration and Time graph, (c) Response Spectrum

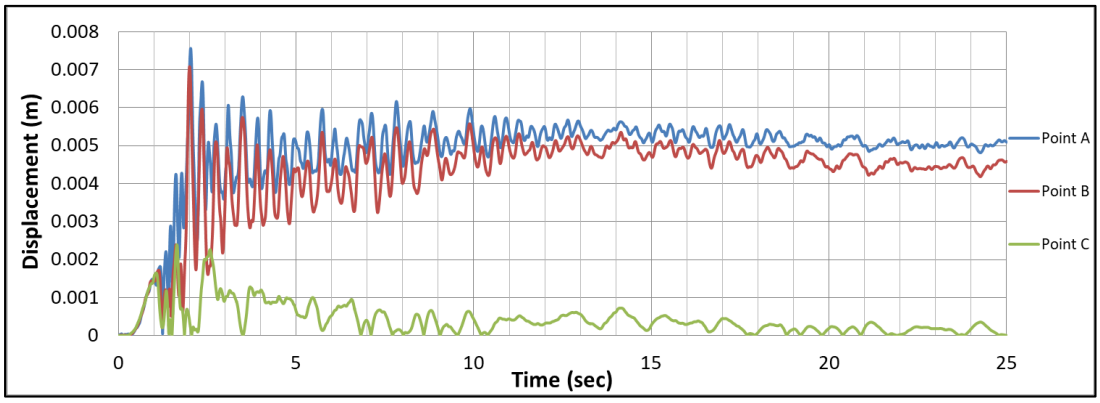

(a)

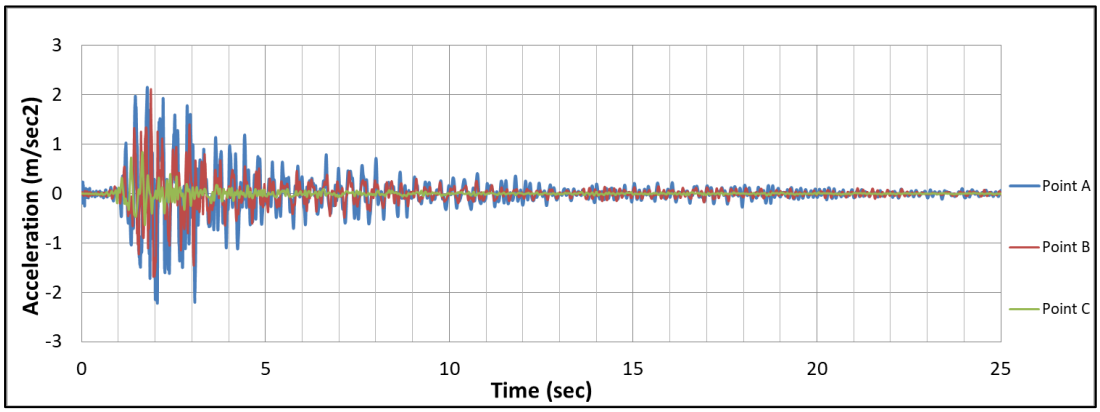

(b)

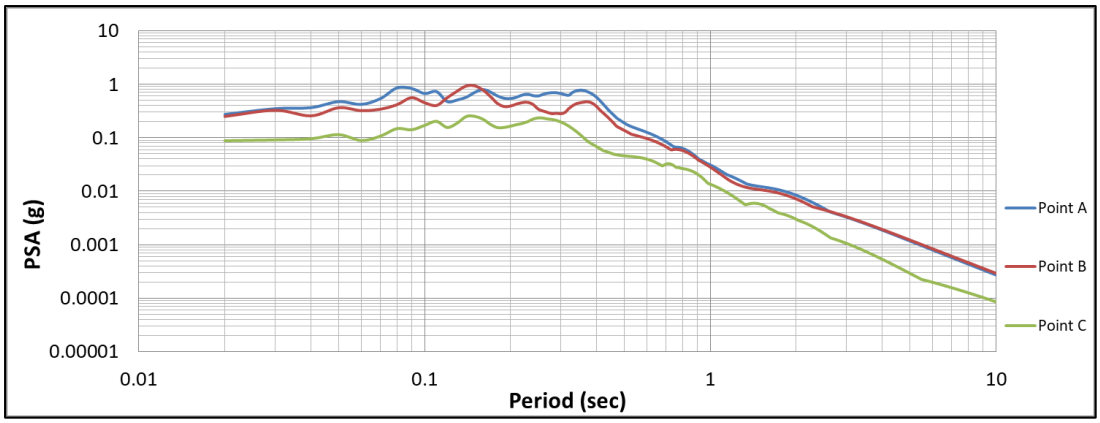

(c)

Figure 3.24 Results graphs of Case # 1b/2c soil model, analysed with RSN# 23_010 ground motion (a) Displacement and Time graph, (b) Acceleration and Time graph, (c) Response Spectrum

CHAPTER 4

INTERPRETATION OF THE ANALYSIS RESULTS

Fully nonlinear, 2-D dynamic numerical analyses are performed in PLAXIS 2D software by utilizing the slope geometries and input ground motions presented in Chapter 3. In total, 2400 analysis are performed as the combination of eight analysis cases with 300 input ground motions. Resultant maximum and final displacements at the centre of gravity of the sliding mass are obtained and utilized as the engineering demand parameters for developing the preliminary prediction models. In this chapter, prediction or seismic demand models for maximum and final displacements based on input ground motion parameters are presented and discussed.

4.1 Preliminary Seismic Demand Models for Slope Displacement

Different ground motion IMs representing the amplitude (PGA, peak ground velocity, PGV or Arias Intensity, I_a), duration (e.g. significant duration), and frequency content (e.g. spectral acceleration at 1.0 sec, mean period) were tested in the previous studies in terms of their correlation with the slope displacements and their sufficiency (for further details, please refer to Chapter 2). Fotopolou and Pitilakis (2015) showed that PGV and I_a have slightly better correlation with the estimated slope displacements when compared to PGA; however, PGA has the superiority over other IMs in terms of hazard compatibility. Therefore, PGA is utilized as the ground motion IM in the preliminary seismic demand models developed in this study. To be able to perform linear regression on the logarithmic terms, the functional form given in Equation 17 is preferred.

$$Log(D) = A + B \times Log(PGA) \mp \epsilon\sigma \qquad \text{(Eq.17)}$$

In Equation 17, D represents the earthquake-induced maximum and permanent slope displacements (in mm), PGA is the maximum acceleration of the input ground motion at the bedrock level (in g), ε is the standard normal variant with zero mean and unit standard deviation, and σ is the standard deviation in log units. Coefficients A and B represent the intercept and the slope of the linear models and they are estimated by linear regression analysis in SPSS software (Version 22, IBM Corp, 2013). Estimated coefficients and the standard deviations of the models for each analysed case for maximum and permanent slope displacements are provided in Table 4.1 and Table 4.2, respectively. Figure 4.1 and Figure 4.2 show that the preferred functional form successfully characterizes the relationship between estimated slope displacements and input PGA both for the maximum and final displacements, except for the cases with very small displacements. For very small displacements (<0.001m), model predictions are smaller than the estimated maximum and final displacements by the numerical analysis. It should be noted that the models provided here are not intended to be used in the prediction of seismic slope displacement; they are built to estimate the standard deviations and to analyse the variation of the standard deviations with respect to slope angle and static factor of safety.

Table 4.1 Coefficients of empirical equation and standard deviations considering maximum displacements

Maximum Displacement							
Case Id	**A**	**B**	**St. Dev. (σ)**	**Case #**	**A**	**B**	**St. Dev. (σ)**
1a	3.469	1.617	0.332	2a	2.951	1.357	0.379
1b	2.900	1.361	0.382	2b	2.905	1.352	0.387
1c	2.745	1.316	0.428	2c	2.900	1.361	0.382
1d	2.598	1.253	0.475	2d	2.879	1.394	0.410
				2e	2.900	1.425	0.428

Table 4.2 Coefficients of empirical equation and standard deviations considering final displacements

Final Displacement							
Case Id	**A**	**B**	**St. Dev. (σ)**	**Case #**	**A**	**B**	**St. Dev. (σ)**
1a	3.586	1.923	0.319	2a	2.896	1.652	0.351
1b	2.872	1.773	0.334	2b	2.809	1.708	0.334
1c	2.660	1.870	0.277	2c	2.872	1.773	0.334
1d	2.348	1.972	0.337	2d	2.880	1.956	0.292
				2e	2.903	2.114	0.369

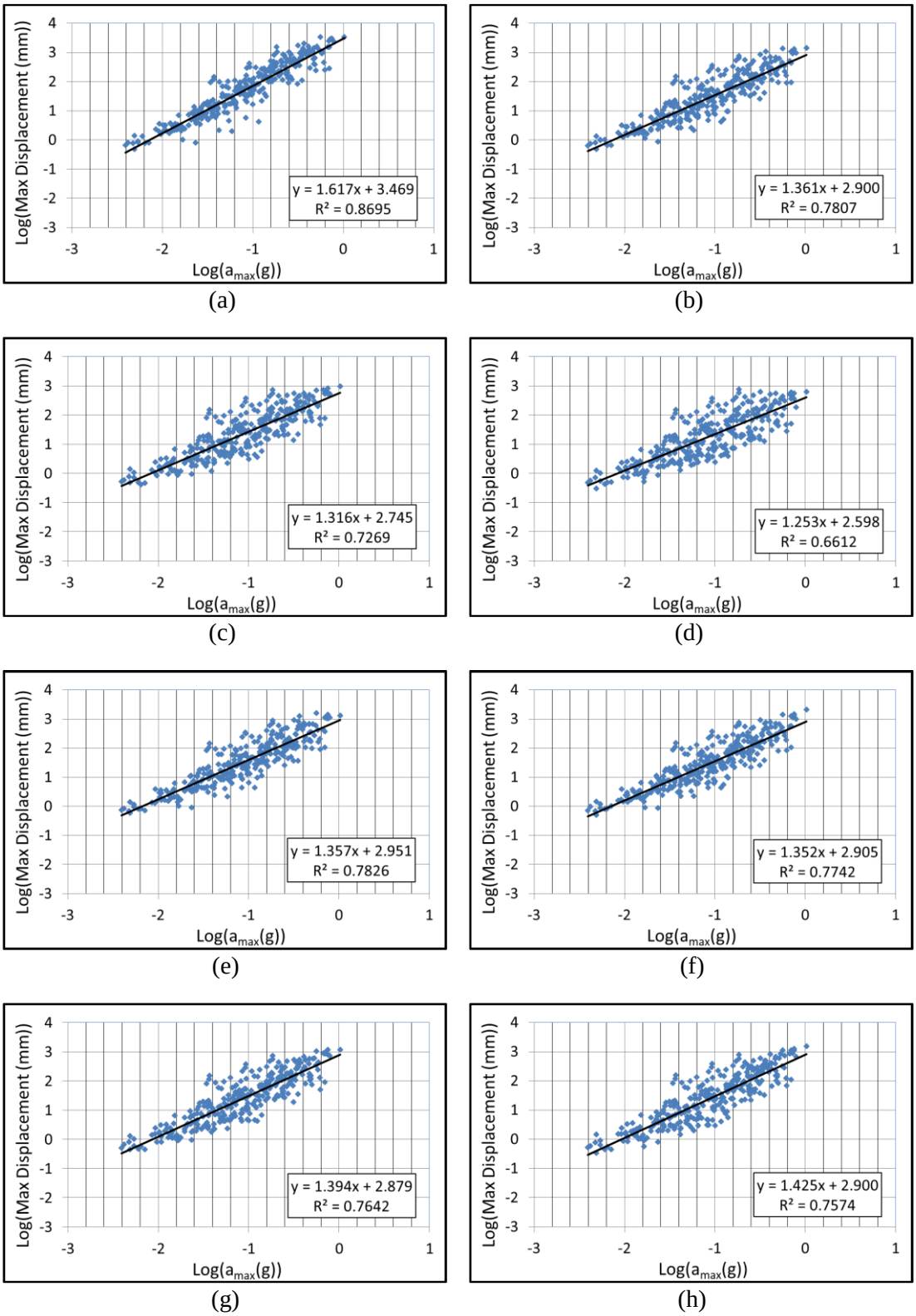

Figure 4.1 Maximum displacement versus input motion PGA plots for (a) Case # 1a, (b) Case # 1b/2c, (c) Case # 1c, (d) Case # 1d, (e) Case # 2a, (f) Case # 2b, (g) Case # 2d and (h) Case # 2e

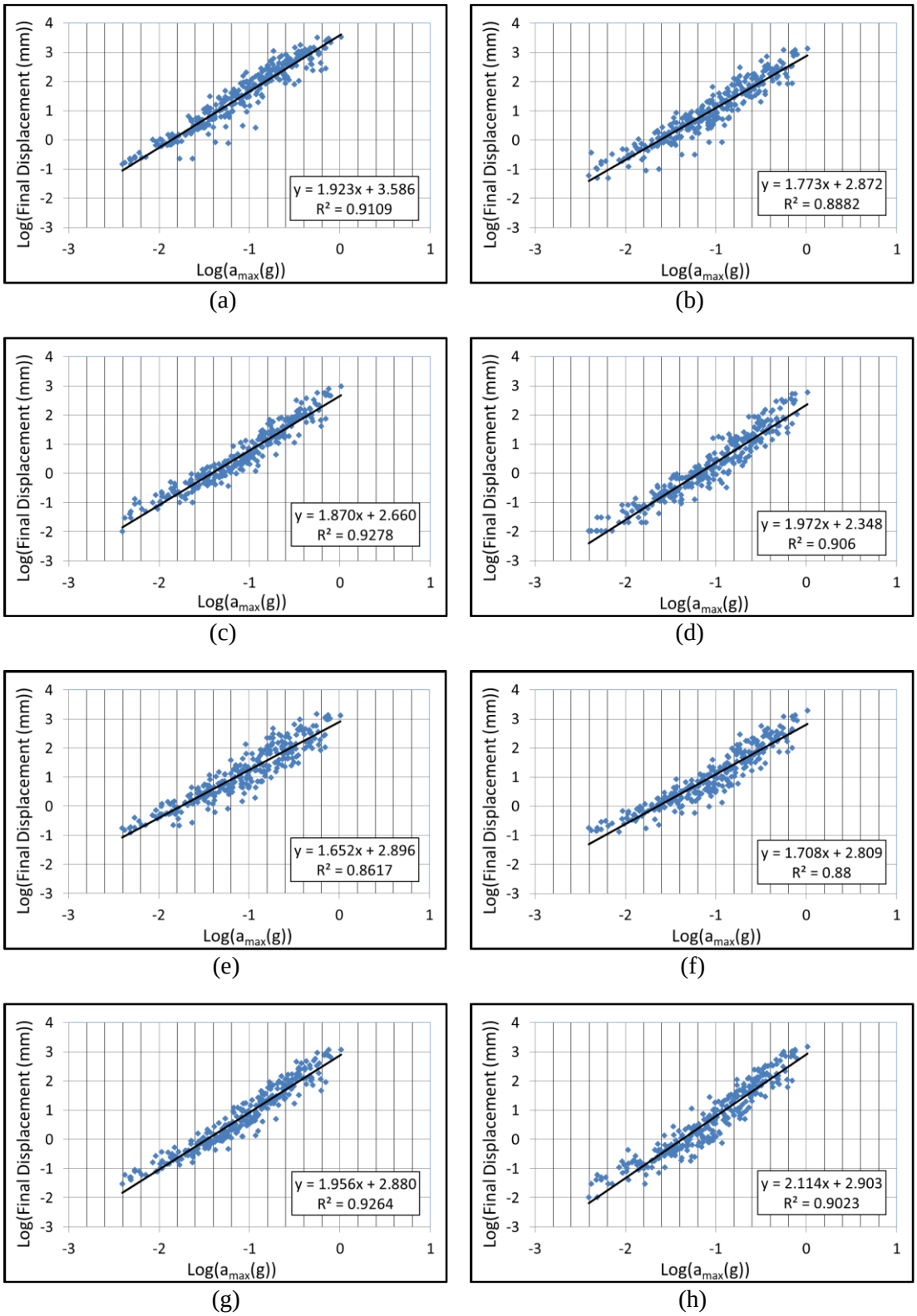

Figure 4.2 Permanent (final) displacement versus input motion PGA plots for (a) Case # 1a, (b) Case # 1b/2c, (c) Case # 1c, (d) Case # 1d, (e) Case # 2a, (f) Case # 2b, (g) Case # 2d and (h) Case # 2e

Figure 4.3 compares the standard deviation of the prediction equation for case # 1b with the mean estimates for low (PGA=0.05 g) and high (PGA=0.4 g) ground shaking levels. When PGA=0.05 g, the mean of the prediction equation is equal to 3.7 mm (0.565 in log units) and the ratio between the mean and the standard deviation is 59%, indicating that the standard deviation is quite high when compared to the final displacements obtained in numerical analyses. When PGA=0.4 g, the mean of the prediction equation is equal to 147 mm (2.166 in log units) and the ratio between the mean and the standard deviation is 15%, therefore standard deviation of the equation is relatively low when compared to the final displacement obtained in numerical analyses.

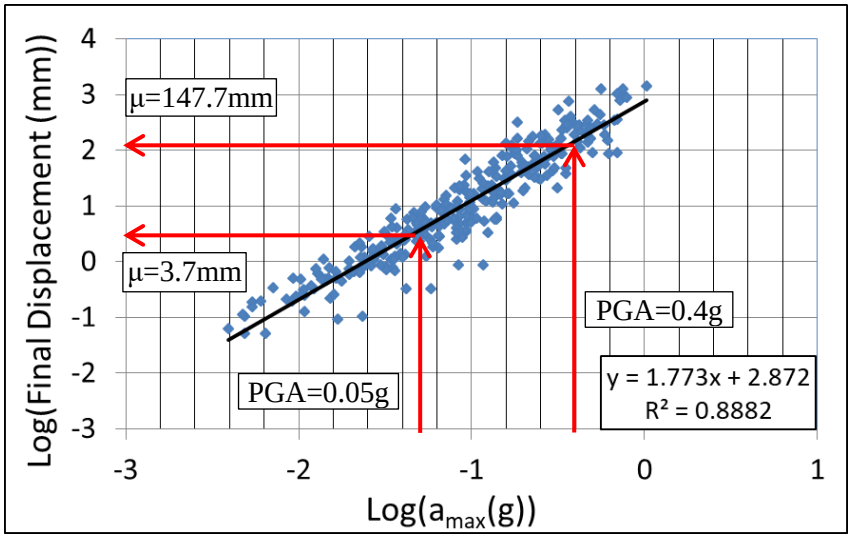

Figure 4.3 Comparison of standard deviation with the mean estimates for Case # 1b for final displacements

4.2 Analysis of Model Residuals

Preliminary seismic demand models are evaluated by examining the distribution of residuals for any potential bias in the model predictions. Residuals values are obtained by subtracting the slope displacements calculated by using the proposed prediction equation from the ones directly obtained in the numerical analysis (in log units). Residuals are plotted with respect to input motion PGA, R_{RUP}, V_{s30} and M_W for maximum and final displacements and provided in Figure 4.4- Figure 4.11. Distribution of residuals are plotted with respect to PGA in Figure 4.4 and Figure 4.5 and these figures do not show any significant trends in the distribution of residuals;

the residuals are centred about the zero line, except for very small ground shaking levels (PGA<0.01g). Because the need for the numerical analysis for such small ground shaking levels is negligible, selected functional form is not modified to account for this underestimation. For some analysis cases, the slope displacements calculated in numerical analysis for very large ground shaking levels (PGA>0.7g) are underestimated by the prediction models. This observation might be related to the limited number of data points at high ground shaking levels; however, due to the limitations of the numerical analysis approach for large displacement values, linear form of the seismic demand model is not altered to account for this slight underestimation. Distribution of residuals with respect to R_{RUP} and V_{s30} are given in Figure 4.6- Figure 4.7 and Figure 4.8- Figure 4.9, respectively. In these plots, no significant trends are observed and the residuals are scattered equally around the zero line. However, for the cases of R_{RUP}>85 km and V_{s30}>1400 m/s, negligible positive or negative trends are observed in the distribution of residuals. This observation might be related to the limited number of data points at high R_{RUP} and V_{s30} values. Figure 4.10 shows that there is a linear trend with M_W in the residuals for maximum slope displacement for almost all of the analyses cases, while this linear trend is not visible in the distribution of residuals for final slope displacement (Figure 4.11). It is possible to add M_W as a predictive parameter in the seismic demand models; however, adding an earthquake parameter to the prediction model might have a negative effect in the hazard compatibility of the prediction model. Additionally, there is only one large magnitude earthquake (1999 Chi-chi earthquake) in the selected dataset and observed underestimation might be related to the characteristics of this event. Because these equations are only preliminary models, possible effect of earthquake magnitude on the model predictions is not considered within the scope of this study.

It is notable that the scatter in the maximum displacement models is more pronounced than the scatter in the final displacement models. Increase in the scatter is also reflected in the estimated standard deviations: the standard deviations for the final displacement prediction models vary between 0.28-0.37, while the standard deviations of the maximum displacement models reach up to 0.475 in log units.

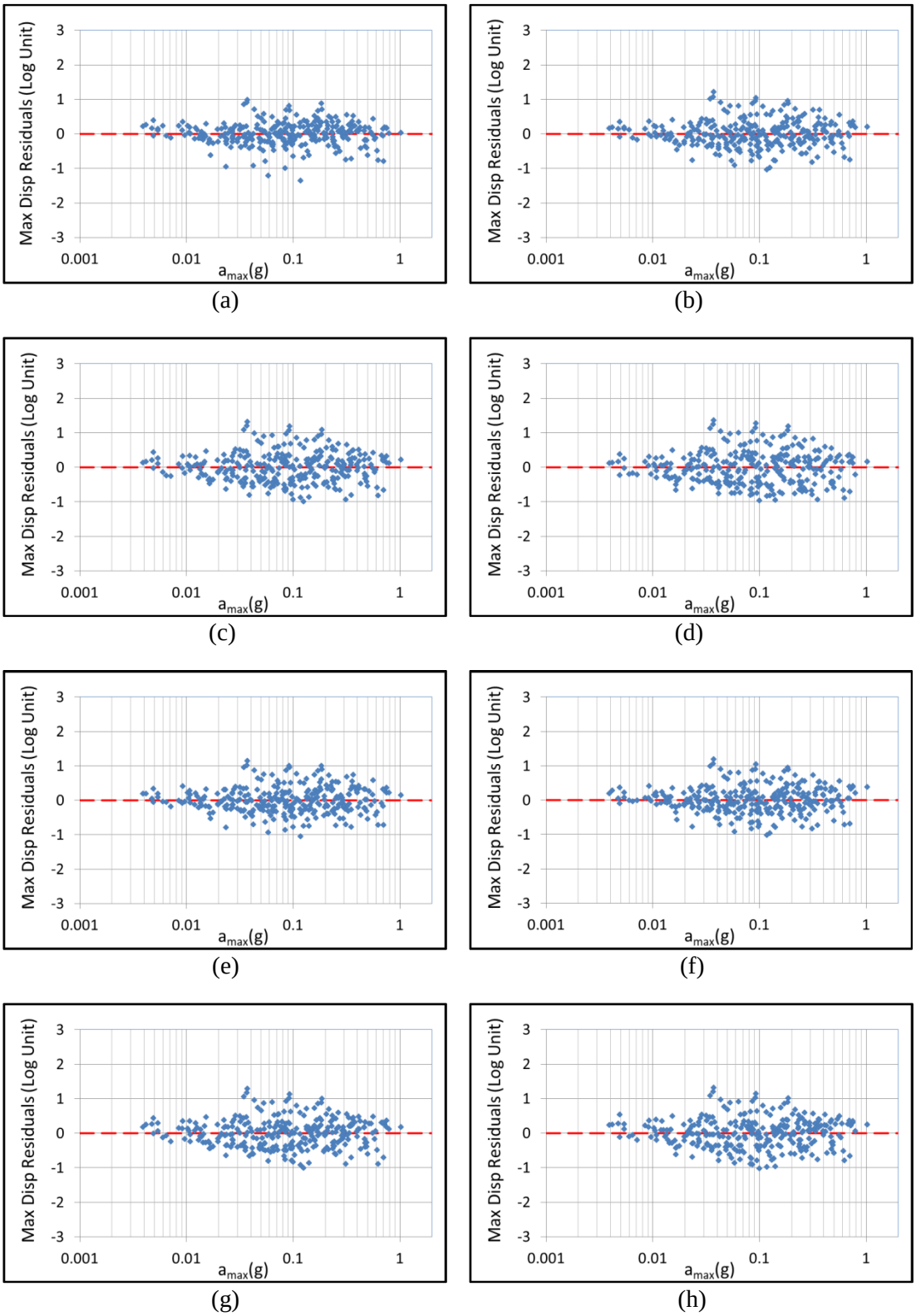

Figure 4.4 Maximum displacement distribution residuals with PGA for models (a) Case # 1a, (b) Case # 1b/2c, (c) Case # 1c, (d) Case # 1d, (e) Case # 2a, (f) Case # 2b, (g) Case # 2d and (h) Case # 2e

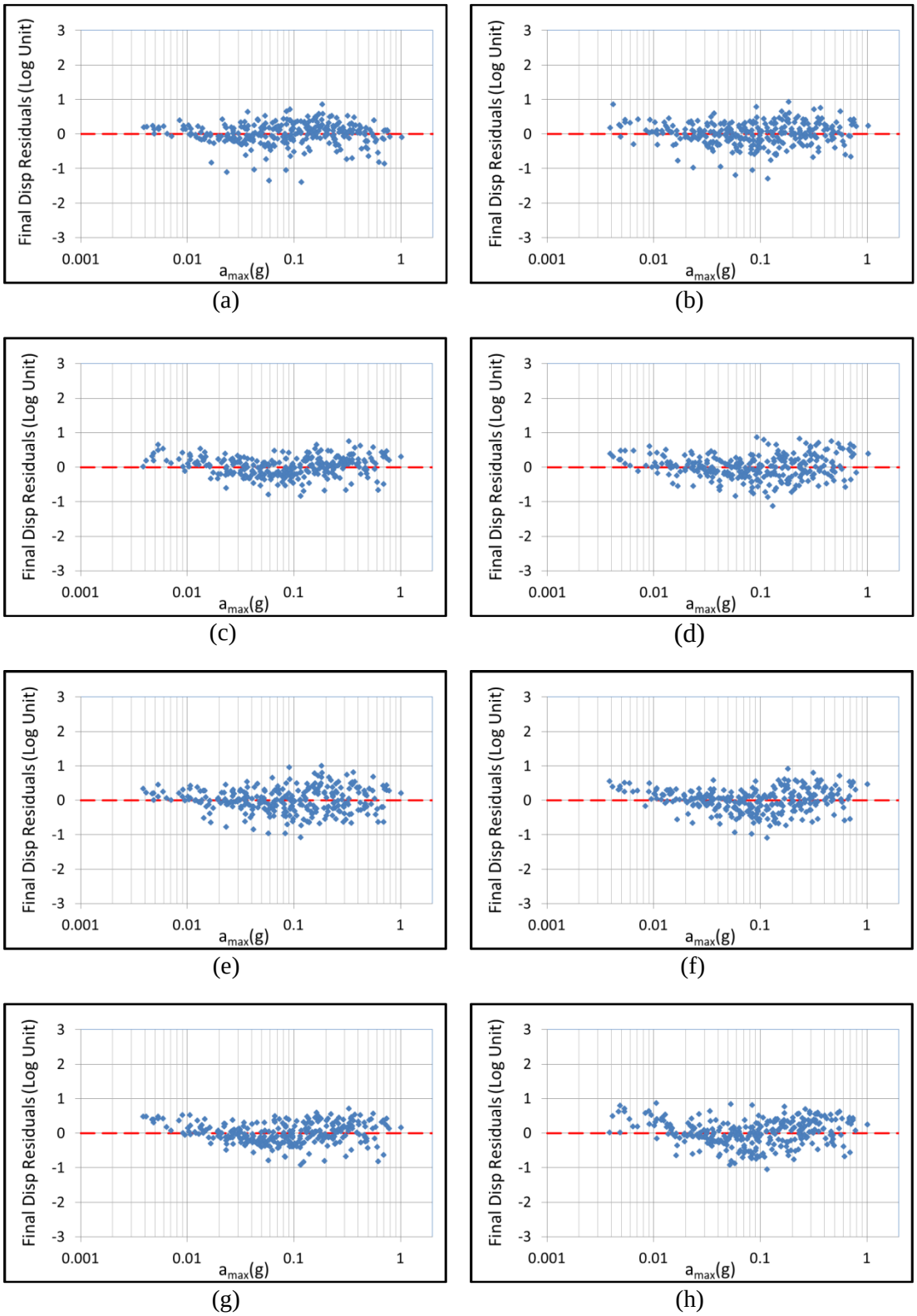

Figure 4.5 Final displacement distribution residuals with PGA for models (a) Case # 1a, (b) Case # 1b/2c, (c) Case # 1c, (d) Case # 1d, (e) Case # 2a, (f) Case # 2b, (g) Case # 2d and (h) Case # 2e

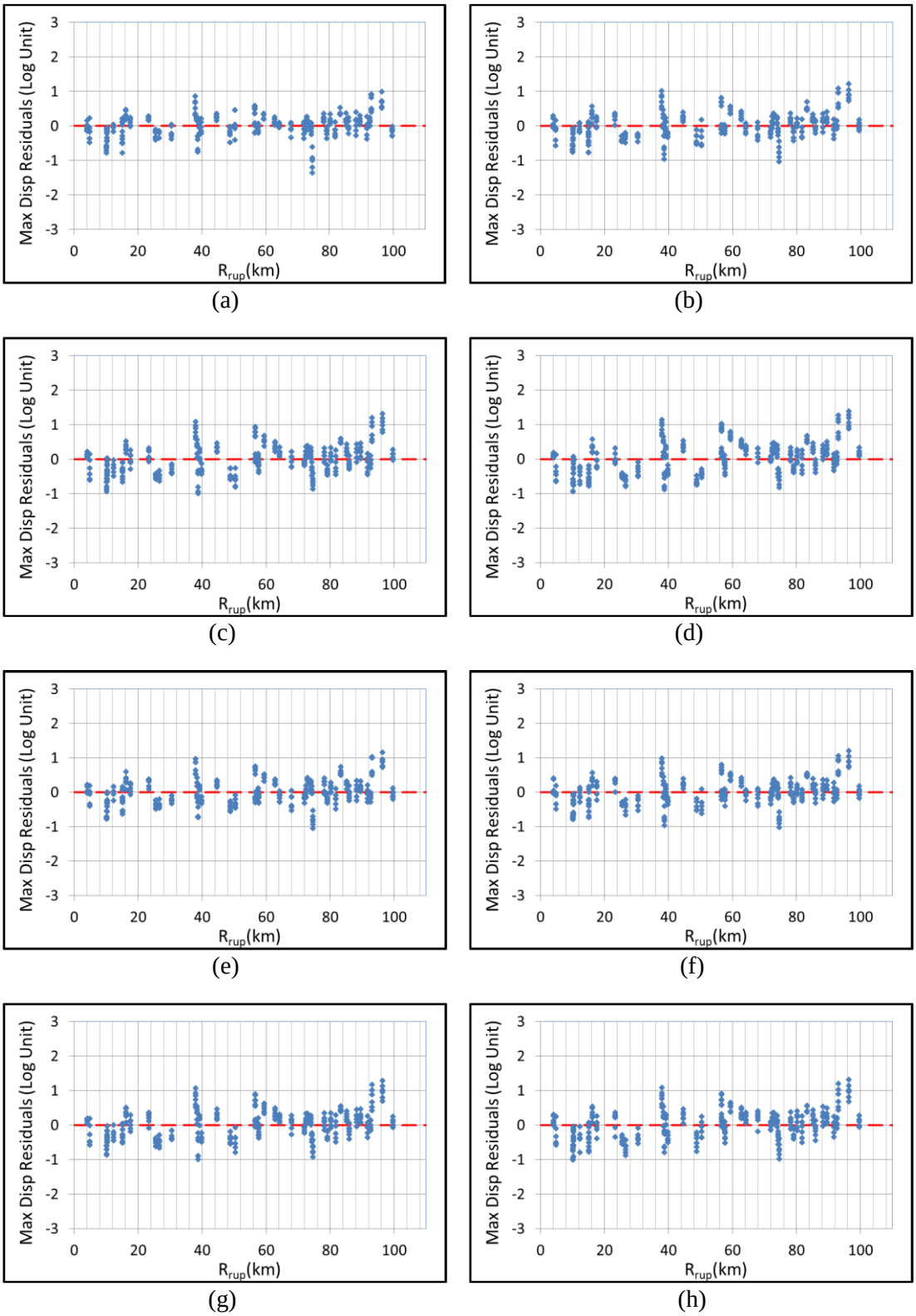

Figure 4.6 Maximum displacement distribution residuals with R_{RUP} for models (a) Case # 1a, (b) Case # 1b/2c, (c) Case # 1c, (d) Case # 1d, (e) Case # 2a, (f) Case # 2b, (g) Case # 2d and (h) Case # 2e

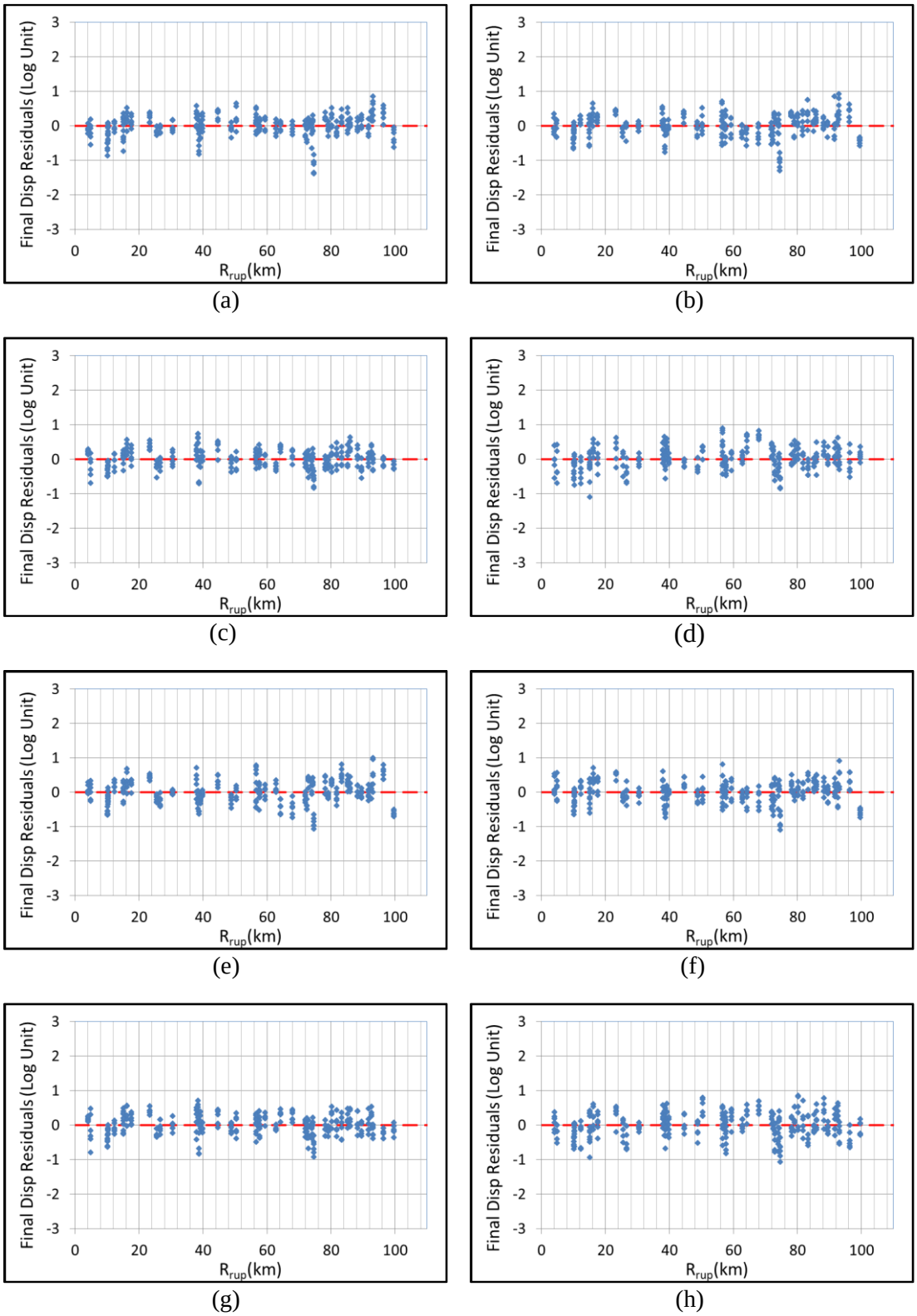

Figure 4.7 Final displacement distribution residuals with R_{RUP} for models (a) Case # 1a, (b) Case # 1b/2c, (c) Case # 1c, (d) Case # 1d, (e) Case # 2a, (f) Case # 2b, (g) Case # 2d and (h) Case # 2e

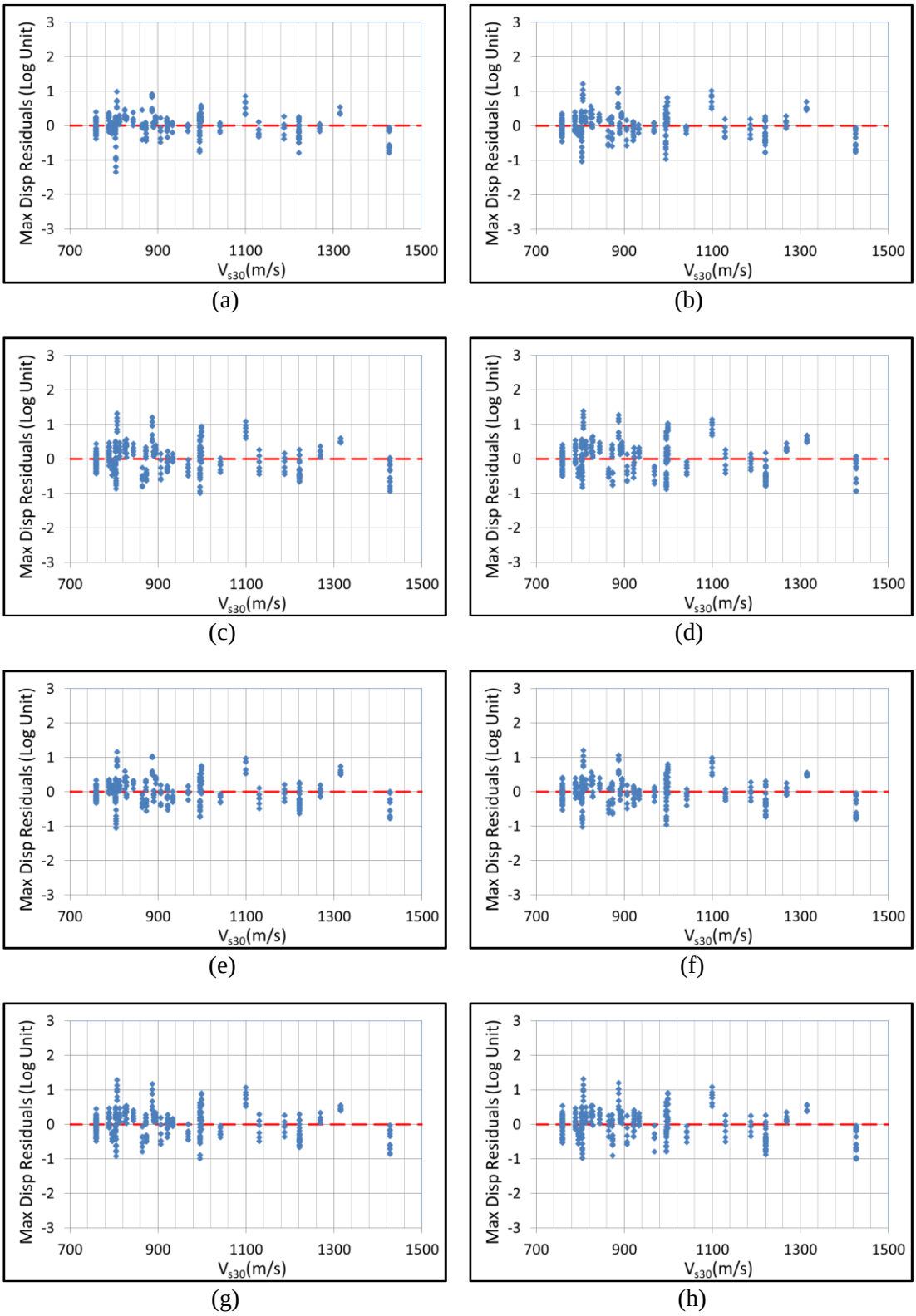

Figure 4.8 Maximum displacement distribution residuals with V_{s30} for models (a) Case # 1a, (b) Case # 1b/2c, (c) Case # 1c, (d) Case # 1d, (e) Case # 2a, (f) Case # 2b, (g) Case # 2d and (h) Case # 2e

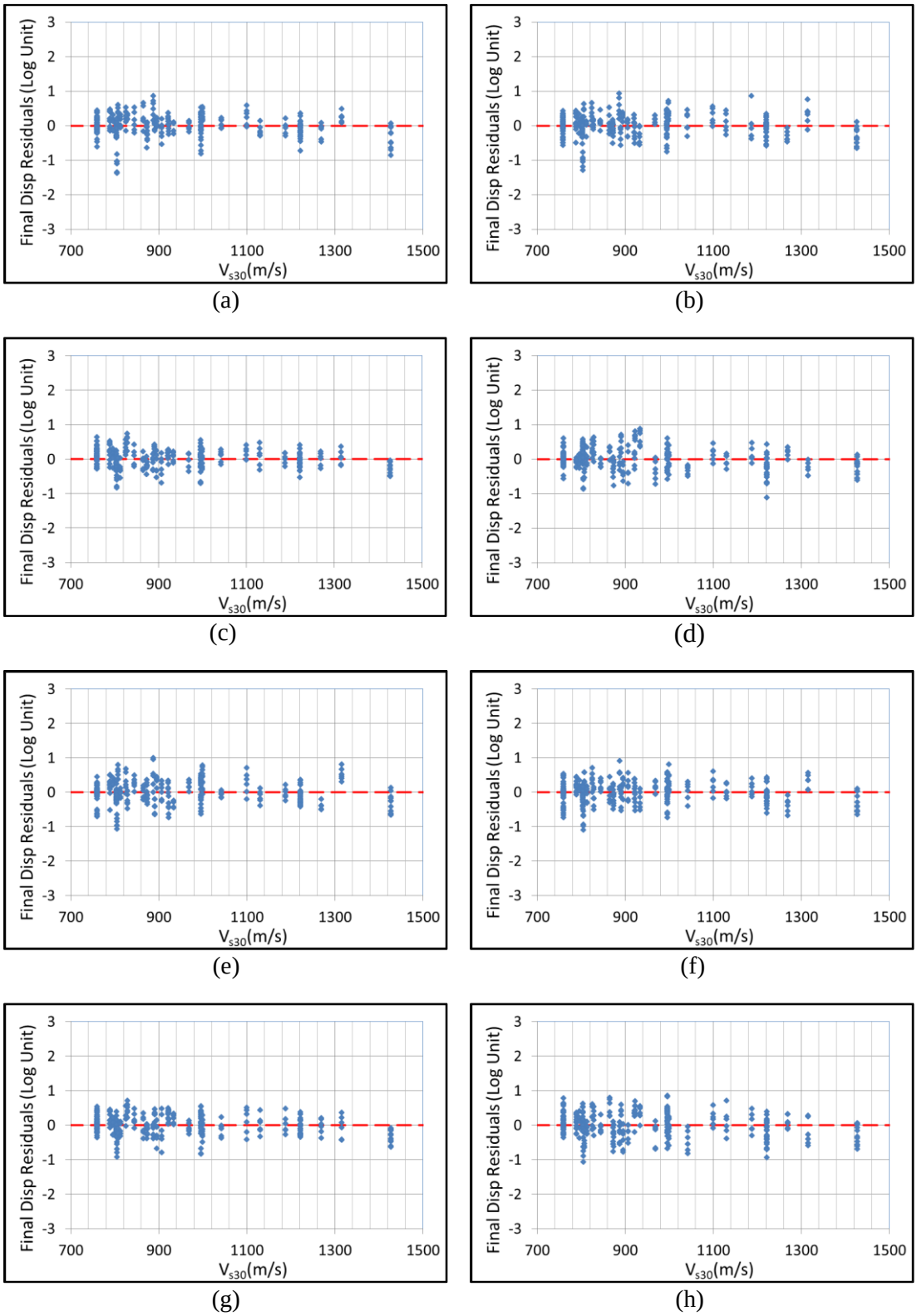

Figure 4.9 Final displacement distribution residuals with V_{s30} for models (a) Case # 1a, (b) Case # 1b/2c, (c) Case # 1c, (d) Case # 1d, (e) Case # 2a, (f) Case # 2b, (g) Case # 2d and (h) Case # 2e

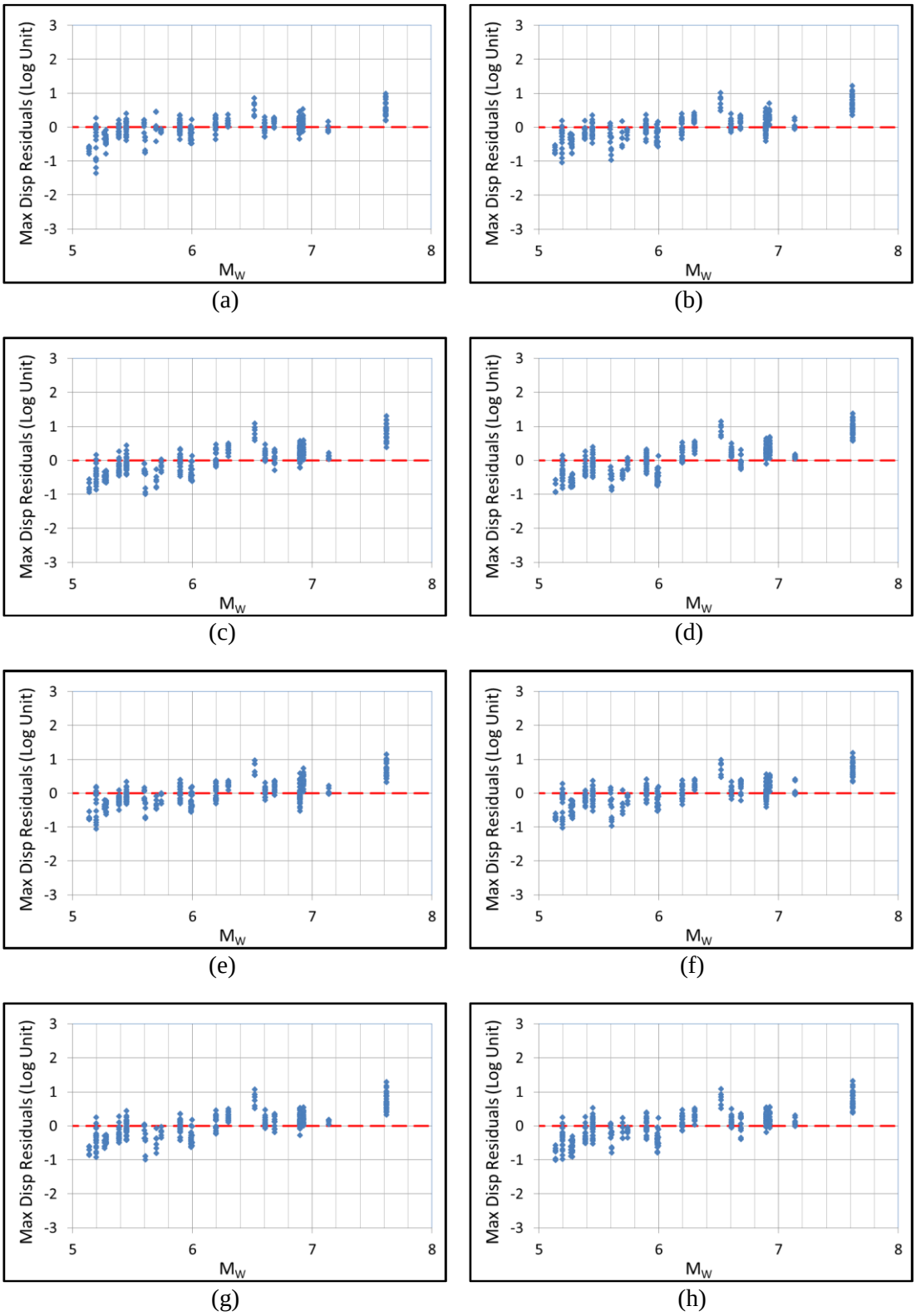

Figure 4.10 Maximum displacement distribution residuals with M_W for models (a) Case # 1a, (b) Case # 1b/2c, (c) Case # 1c, (d) Case # 1d, (e) Case # 2a, (f) Case # 2b, (g) Case # 2d and (h) Case # 2e

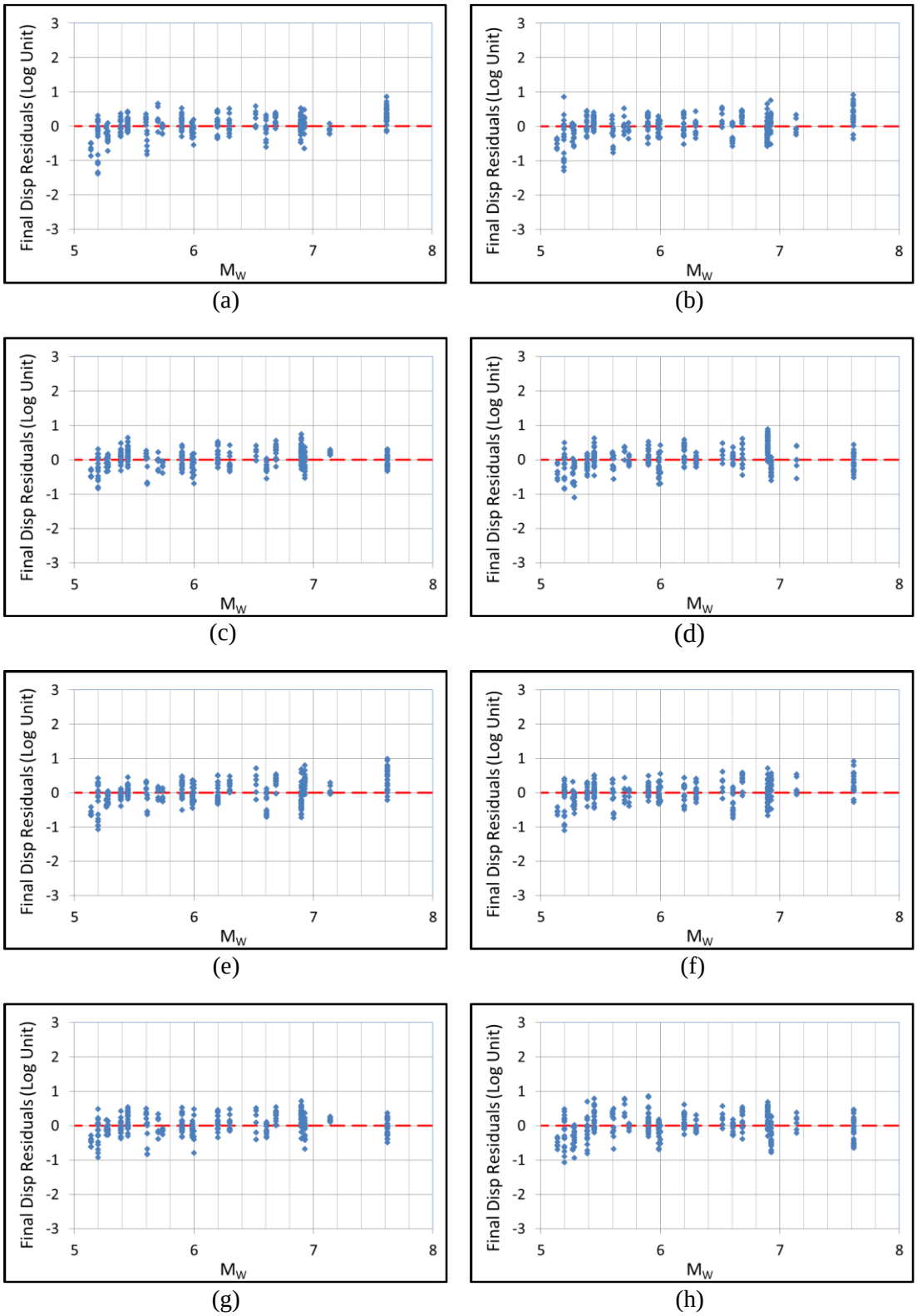

Figure 4.11 Final displacement distribution residuals with M_W for models (a) Case # 1a, (b) Case # 1b/2c, (c) Case # 1c, (d) Case # 1d, (e) Case # 2a, (f) Case # 2b, (g) Case # 2d and (h) Case # 2e

CHAPTER 5

SUMMARY AND CONCLUSIONS

Probabilistic seismic demand models for earthquake-induced slope displacements have the potential of being used for estimating the permanent displacements in natural slopes, dams, and embankments during the earthquakes. However, these models are often associated with a high degree of uncertainty, resulting from the inherent variability in the input ground motions or from the variability in the geotechnical properties of the slope. The main objectives of this study are: (i) to model the variability in the earthquake-induced soil slope displacements that are estimated in numerical analysis due to the selection of input ground motions, (ii) to evaluate the relationship between this variability and the slope properties, and (iii) to select a limited subset of ground motions that represent the median relationship between the input motion PGA and slope displacements.

To achieve these goals, a careful numerical analysis scheme is designed. The input ground motions that represent the rock site conditions and the median response for that particular earthquake scenario are chosen. Considering that the factor of safety in static condition is a parameter, which represents the geotechnical properties of the slope, the effective soil shear strength parameters of the analysed cases are constrained by the factor of safety in static condition and slope angle. In other words, arbitrary slope geometries that have the factor of safety in static condition varying between 1.2 and 2.4 are built and combined with the selected input ground motions for dynamic numerical analysis. Geotechnical engineering parameters required for the dynamic analysis (e.g. Young's modulus, shear modulus, shear wave velocity) are assigned carefully to ensure that these parameters are compatible with the effective shear strength parameters. 2400 dynamic analysis are performed in

PLAXIS 2D software, combining eight different slopes in dry (drained) soil with 300 input ground motions. The centre of gravity for the displaced mass in the static safety analysis is determined for each case, and the resultant maximum and permanent displacements at that point is recorded in each dynamic analysis. It should be noted that centre of gravity of the displacement contours in the dynamic analysis stage could be different from the selected point; however, this difference is ignored in this study.

In order to quantify the variability in estimated slope displacements due to input ground motions, simple empirical prediction models are developed for maximum and permanent displacements using linear regression. PGA is chosen as the ground motion IM for the prediction equation, because of its sufficiency and hazard compatibility. A linear functional form in log-log space is preferred for simplicity because the sole reason for developing these preliminary models is to estimate the standard deviations. Even though considering other functional forms and adding other ground motion IMs in the probabilistic seismic demand models for earthquake-induced slope displacements may result in smaller standard deviations, these simplified fits to the data points are preferred because they seem to properly display the relation between slope displacements and input motion PGA according to Figure 4.1 and Figure 4.2. Except for the cases with very small (PGA<0.01g) and very large (PGA>0.7g) ground shaking levels, the relationship between the input PGA and slope displacements are linear in log-log space. The model residuals with the input motion PGA, R_{RUP} and V_{s30} show no systematic bias in the estimations. However, there is a linear trend with M_W in the residuals only for maximum displacements (not for final displacements).

Variation of the standard deviation of the empirical prediction models for the maximum and permanent slope displacements with the static factor of safety and the slope angle is presented in Figure 5.1 and Figure 5.2, respectively. Both figures show that the standard deviation of the permanent slope displacement models does not fluctuate significantly with static factor of safety or slope angle. The standard deviation value varies between 0.27 and 0.37 in log units; however, it does not systematically increase with increasing slope angle or decreasing factor of safety.

For the case of maximum slope displacement models, the variation of the standard deviation with slope angle is also not significant and no systematic trends are observed in Figure 5.2. However, a positive trend in the standard deviations (increase from 0.33 to 0.47 in log units) with increasing factor of safety is visible for maximum slope displacements in Figure 5.1. This observation suggest that when the slope is close to the failure in static conditions, the maximum displacement values are relatively less dependent on the selected input motion; while for the cases with high static factor of safety, the scatter in the maximum displacement values increase.

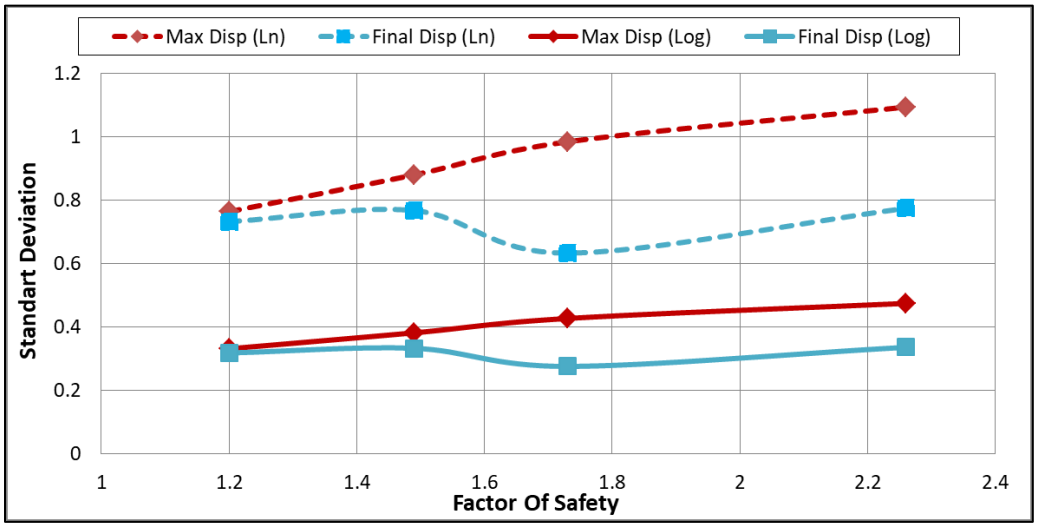

Figure 5.1 Variation of the standard deviation of the preliminary seismic demand models with factor of safety in static condition

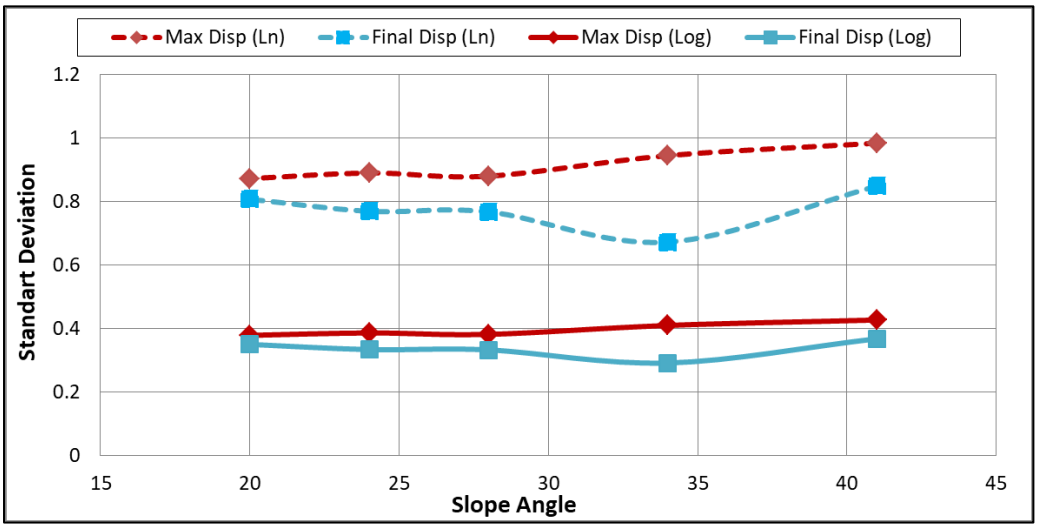

Figure 5.2 Variation of the standard deviation of the preliminary seismic demand models with slope angle

The standard deviations proposed in this study (0.6 – 0.8 in Ln units) are smaller than the standard deviations given in previous attempts (e.g. Fotopoulou and Pitilakis, 2015 suggested 0.93 in Ln units). The reduction in the standard deviations is related to the applied ground motion selection procedure: the ground motions that are significantly different from the median spectrum for a particular scenario were eliminated from the candidate ground motion list. This decision reduced the standard deviations of the models approximately by 10-15%, even if the selected ground motions were multiplied with relatively high scale factors (up to SF=5).

5.1 Final Subset of Recordings for Dynamic Numerical Analysis

The final goal of this study is to propose a limited set of ground motions that might be preferred in future studies because they represent the median relationship between the input PGA and permanent slope displacement. For this purpose, a percentage difference (PD) is defined using the actual values of permanent displacement obtained from the numerical analysis and the predicted permanent displacement values based on the proposed models as shown in Equation 18:

$$\%\ Diff. = \frac{|Actual\ permanent\ disp. - Predicted\ permanent\ disp.|}{Actual\ permanent\ disp.} \times 100 \qquad \text{(Eq.18)}$$

This index represents the closeness of the actual slope displacements to the median predictions of the model. Value of the PD is calculated for each ground motion for each analysed slope case and the average value of the PDs from eight prediction models is assigned to the ground motion recordings. Initially, the ground motions with average PD bigger than 50% is eliminated. Remaining ground motions is sorted according to their average PD values and checked for the consistency of average PD value with scaling: a ground motion recording is considered eligible if the original and scaled (both with 2.5 and 5) versions have small average PD values. Finally, ground motions with both orthogonal components have small average PD values are determined. Eventually, 6 orthogonal horizontal pairs are selected for the final subset as shown in Table 5.1 (RSN# 59, 146, 643, 3318, 8707, 8819), because both horizontal components might be required in three dimensional numerical analysis. Considering that the number of selected recordings may need to be higher than 12

individual recordings or 6 ground motion pairs according to the earthquake codes and regulations, 6 additional ground motions with very small average PD values are added to the final list (Table 5.1, RSN# 23, 680, 797, 1011, 1715, 5649). The selected subset of recordings consists of motions from R_{RUP}, varying from 10.67 to 89.72 km. the PGA values range from 0.015 to 0.795 g.

The regression analysis is repeated using only the selected subset of recordings to understand if the median lines from the new regression are consistent with the median lines determined using the full dataset. Figure 5.3 shows that median lines based on the selected subset of recordings (red dashed lines) are very close to the median lines (black lines) determined with the full set of recordings. Therefore, the selected subset of recordings properly represents the median relationship between the input motion PGA and permanent slope displacements.

Distribution of the selected subset of recordings with magnitude, distance, V_{S30}, and fault mechanism is given Figure 5.4, in comparison with the initial dataset. Figure 5.4(a) shows that all of the large magnitude earthquakes (M_w>7) of the initial dataset are eliminated because of high average PD values. Distribution of the recordings with distance is still uniform, except for large distances (Figure 5.4b). Most of the large distance recordings (R_{rup}>75km) of the initial dataset are excluded from the selected subset. According to Figure 5.4(c), half of the recordings from stiff rock sites (V_{s30}>1100m/s) are included in the final subset; while, majority of the recordings with V_{s30}<1100m/s are eliminated. There is only one recording from normal events in the initial database; however, this recording is not included in the final subset of recordings. Distribution of recordings among reverse, reverse/oblique, and strike slip earthquake mechanism is nearly uniform (Figure 5.4d). The list of recordings given in Table 5.1 is the most significant contribution of this study. These acceleration-time histories may be preferred in the numerical dynamic analysis to examine slope displacements and when the median estimates of these recordings are combined with the standard deviations given in this study, the centre, body and the range in probabilistic seismic demand models for earthquake-induced slope displacements may be properly modelled.

Table 5.1 Selected strong ground motions for future studies

PEER Record Sequence Number	Earthquake Name	Magnitude (M_w)	Mechanism	R_{jb}(km)	R_{rup}(km)	V_s^{30}(m/sec)	PEER Record Name for Horizontal Component 1*	PEER Record Name for Horizontal Component 2*
23	San Francisco	5.28	Reverse	9.74	11.02	874.72	N/A	RSN23_SANFRAN_GGP100.AT2
59	San Fernando	6.61	Reverse	89.37	89.72	813.48	RSN59_SFERN_CSM095.AT2	RSN59_SFERN_CSM185.AT2
146	Coyote Lake	5.74	strike slip	10.21	10.67	1428.14	RSN146_COYOTELK_G01230.AT2	RSN146_COYOTELK_G01320.AT2
643	Whittier Narrows-01	5.99	Reverse Oblique	23.4	27.64	1222.52	RSN643_WHITTIER.A_A-WON075.AT2	RSN643_WHITTIER.A_A-WON165.AT2
680	Whittier Narrows-01	5.99	Reverse Oblique	6.78	18.12	969.07	N/A	RSN680_WHITTIER.A_A-KRE360.AT2
797	Loma Prieta	6.93	Reverse Oblique	74.04	74.14	873.1	RSN797_LOMAP_RIN000.AT2	N/A
1011	Northridge-01	6.69	Reverse	15.11	20.29	1222.52	N/A	RSN1011_NORTHR_WON185.AT2
1715	Northridge-06	5.28	Reverse	13.15	17.14	1222.52	N/A	RSN1715_NORTH392_WON185.AT2
3318	Chi-Chi_ Taiwan-06	6.3	Reverse	62.46	63.26	804.36	RSN3318_CHICHI.06_CHY102N.AT2	RSN3318_CHICHI.06_CHY102E.AT2
5649	Iwate_ Japan	6.9	Reverse	72.44	72.44	1269.78	N/A	RSN5649_IWATE_IWTH17EW.AT2
8707	40204628	5.45	strike slip	30.45	30.75	760	RSN8707_40204628_NCJUMHNN.AT2	RSN8707_40204628_NCJUMHNE.AT2
8819	14383980	5.39	Reverse Oblique	38.48	41.17	760	RSN8819_14383980_CIMWCHNN.AT2	RSN8819_14383980_CIMWCHNE.AT2

*Record name with N/A are eliminated during selection process due to the selection criteria

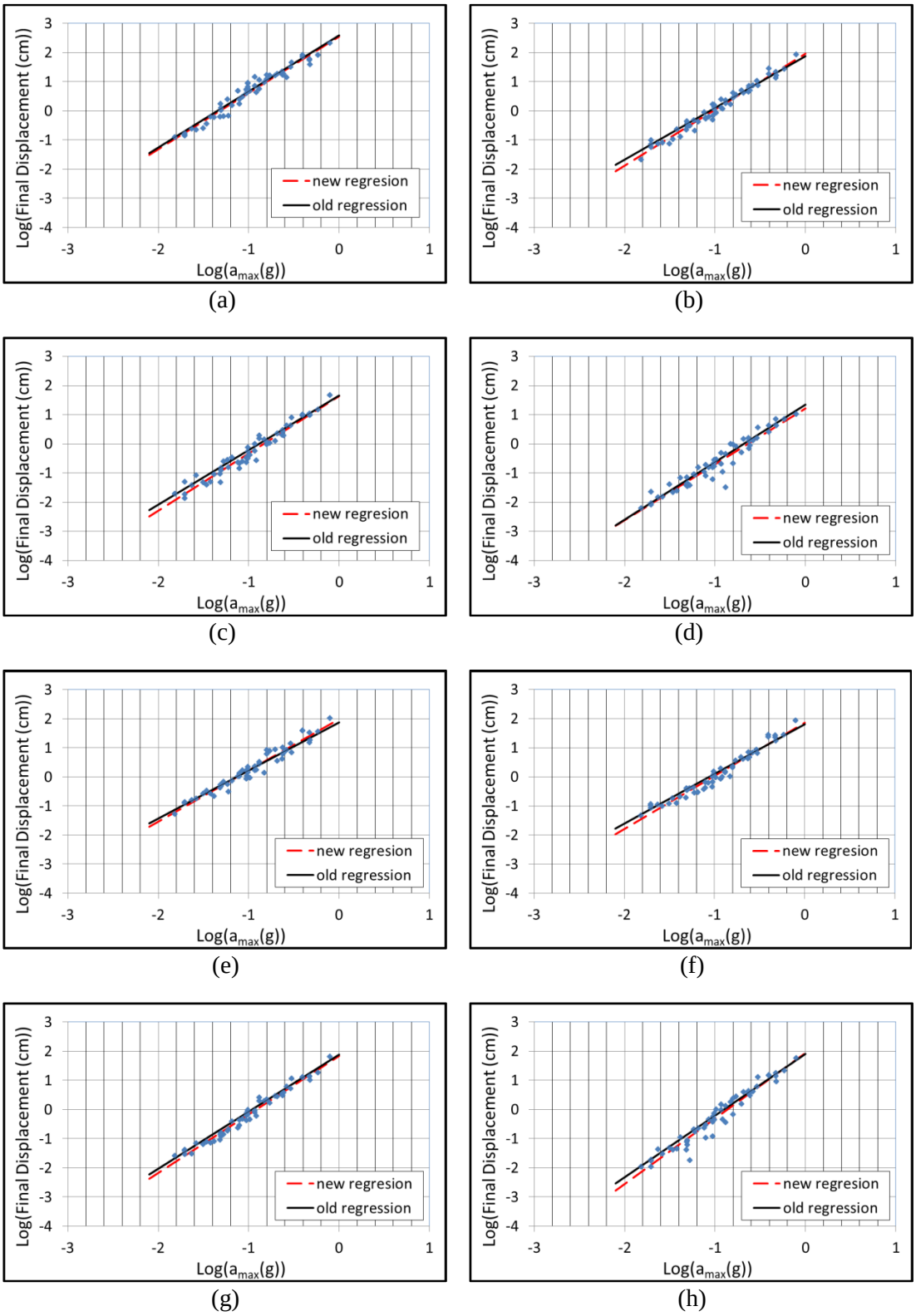

Figure 5.3 Comparison of the regressed line final displacement based on the full dataset and the selected subset of recordings for: (a) Case # 1a, (b) Case # 1b/2c, (c) Case # 1c, (d) Case # 1d, (e) Case # 2a, (f) Case # 2b, (g) Case # 2d and (h) Case # 2e

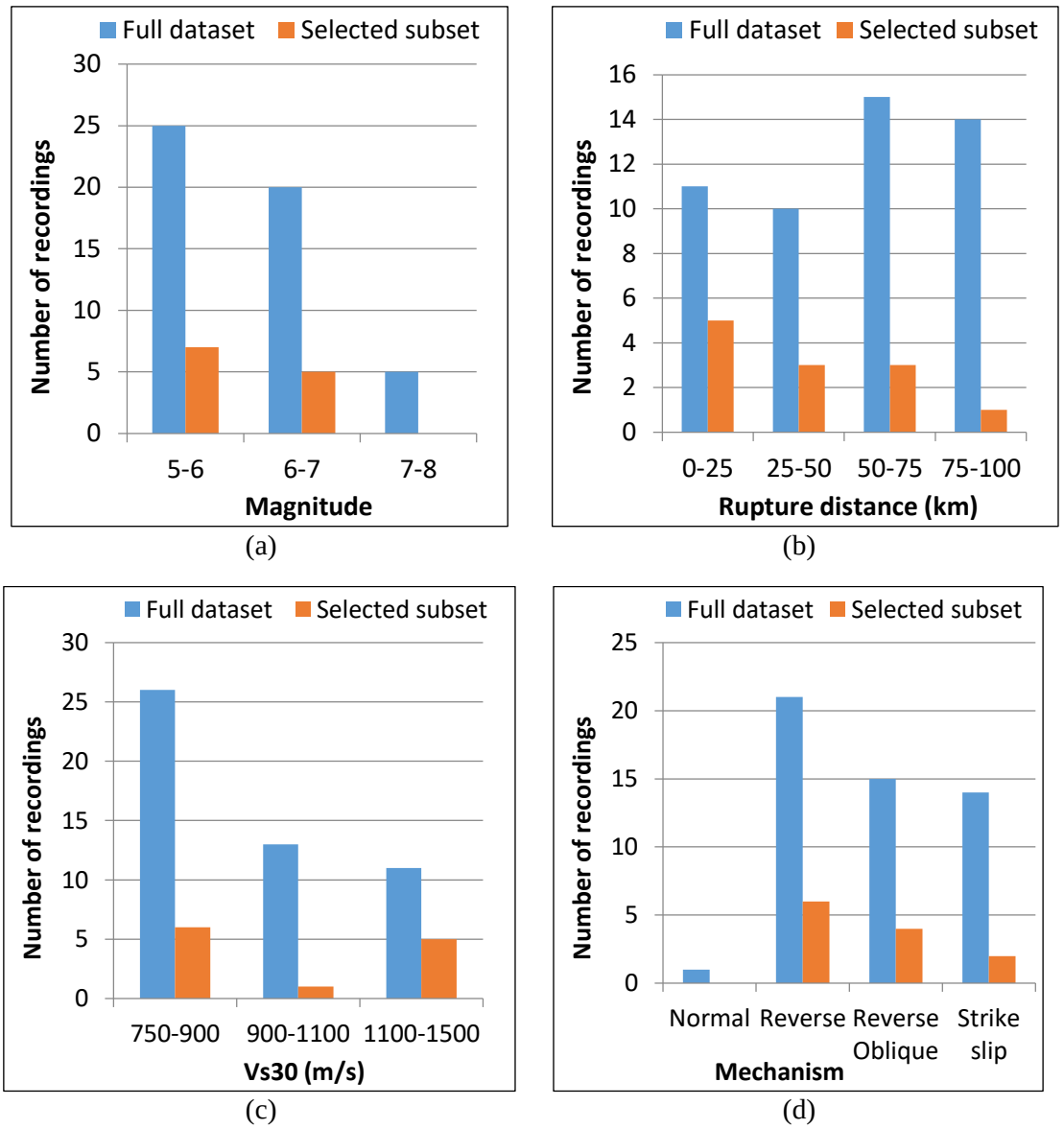

Figure 5.4 Distribution of the recordings in the initial dataset and the final subset with (a) magnitude, (b) rupture distance, (c) V_{S30}, and (d) fault mechanism

5.2 Limitations of This Study and Recommendations for Future Studies

Due to time considerations, the numeric analyses were limited with only eight slope geometries combined with dry (drained) soil cases within the scope of this study. In other words, undrained slope stability analyses were not performed for static conditions and the effect of water table was not considered on the slope displacements estimated in dynamic analyses. The mean estimates of the developed prediction models would be different from the slope displacements expected for undrained conditions. To understand if the standard deviations will also be different

for the undrained soil or rock conditions, further analyses with various water table levels can be performed in future studies.

Simple preliminary seismic demand models developed in this study can be improved by more advanced ones in the future studies, by using additional IMs or by changing the functional form of equation, which may lead to a reduction in the standard deviations. Especially, adding a term that includes M_W may improve the prediction performance of the models. It should be noted that using the current prediction models may result in the underestimation of maximum displacements for large magnitude (M_W>7) events and overestimation of maximum displacements for small magnitude (M_W<5.5) events. Selected subset of recordings is lack of ground motions from large magnitude earthquakes. Considering that there is a trend in the model residuals with respect to M_W, additional recordings from large magnitude events might be added to the subset if earthquake scenarios M_W>7 is critical for design. Additional recordings from normal earthquakes might be added to selected subset of recordings, for the cases with significant ground motion contribution from normal earthquakes (e.g. Western Anatolia).

REFERENCES

Abrahamson, N., & Silva, W. (2008). Summary of the Abrahamson & Silva NGA ground-motion relations. Earthquake spectra, 24(1), 67-97.

Abramson, L. W., Lee, T. S., Sharma, S., & Boyce, G. M. (2002). Slope stability and stabilization methods. John Wiley & Sons.

Akbaş, B., Gülerce, Z., Kalpakçı, V., and Süzen, M. L. Seismic Demand Models for Estimating the Pseudo-Static Factor of Safety for Slope Failure, Proceedings of 16th European Conference on Earthquake Engineering (16ECEE), 18-21 June 2018, Thessaloniki, Greece.

American Geophysical Union. (2009, March 12). Wenchuan Earthquake Mudslides Emit Greenhouse Gas. ScienceDaily. Retrieved March 27, 2019 from www.sciencedaily.com, last visited on March 2016

Athanasopoulos-Zekkos, A., Pence, H., & Lobbestael, A. (2016). Ground motion selection for seismic slope displacement evaluation analysis of earthen levees. Earthquake Spectra, 32(1), 217-237.

Brinkgreve, R. B. J., Kappert, M. H., & Bonnier, P. G. (2007). Hysteretic damping in a small-strain stiffness model. Proc. of Num. Mod. in Geomech., NUMOG X, Rhodes, 737-42.

Building Seismic Safety Council (2004). NEHRP Recommended Provisions for seismic regulations for new buildings and other structures (FEMA 450), Building Seismic Safety Council, National Institute of Building Sciences, Washington D.C.

Cundall, P. A., Hansteen, H., Lacasse, S., & Selnes, P. B. (1980). NESSI, soil structure interaction program for dynamic and static problems. Norwegian Geotechnical Institute, Report, 51508-9.

Das B.M. (1985). “Advanced Soil Mechanics” Mc-Graw Hill.

Dos Santos, J. A., & Correia, A. G. (2001). Reference threshold shear strain of soil. Its application to obtain an unique strain-dependent shear modulus curve for soil. In Proceedings of The International Conference on Soil Mechanics and Geotechnical Engineering, Vol. 1, pp. 267-270.

Duncan, J. M., & Chang, C. Y. (1970). Nonlinear analysis of stress and strain in soils. Journal of Soil Mechanics & Foundations Div. ASCE, 96: 1629-1653.

Dutta, S. C., & Roy, R. (2002). A critical review on idealization and modeling for interaction among soil–foundation–structure system. Computers & structures, 80(20-21), 1579-1594.

Elgamal, A. W. M., Scott, R. F., Succarieh, M. F., & Yan, L. (1990). La Villita dam response during five earthquakes including permanent deformation. Journal of Geotechnical Engineering, 116(10), 1443-1462.

Erol, A. O., & Çekinmez, Z. (2014). Geoteknik mühendisliğinde saha deneyleri. Yüksel Proje Yayınları.

Fan, X., Juang, C. H., Wasowski, J., Huang, R., Xu, Q., Scaringi, G., ... & Havenith, H. B. (2018). What we have learned from the 2008 Wenchuan Earthquake and its aftermath: A decade of research and challenges. Engineering geology, 241, 25-32.

FHWA-IF-02-034 (2002a). "Geotechnical Engineering Circular No.5: Evaluation of Soil and Rock Properties" Federal Highway Administration, U.S. Department of Transportation.

Fotopoulou, S. D., & Pitilakis, K. D. (2015). Predictive relationships for seismically induced slope displacements using numerical analysis results. Bulletin of Earthquake Engineering, 13(11), 3207-3238.

Griffiths, D. V., & Prevost, J. H. (1988). Two-and three-dimensional dynamic finite element analyses of the Long Valley Dam. National Center for Earthquake Engineering Research.

Gülerce, Z., & Balal, O. (2017). Probabilistic seismic hazard assessment for sliding displacement of slopes: An application in Turkey. Bulletin of Earthquake Engineering, 15(7), 2737-2760.

Imai, T., Fumoto, H., & Yokota, K. (1976). P-and S-wave velocities in subsurface layers of ground in Japan. Urawa Research Inst., Oyo Corporation.

Jibson, R. W. (1993). Predicting earthquake-induced landslide displacements using Newmark's sliding block analysis. Transportation research record, 1411, 9-17.

Jibson, R. W. (2011). Methods for assessing the stability of slopes during earthquakes—A retrospective. Engineering Geology, 122(1-2), 43-50.

Journal of the Indian Express. "Landslide After Massive Nepal Earthquake Caught on Camera", www. indianexpress.com, last visited on March 2016

Kottke, A., & Rathje, E. M. (2008). A semi-automated procedure for selecting and scaling recorded earthquake motions for dynamic analysis. Earthquake Spectra, 24(4), 911-932.

Kramer, S.L., 1996. Geotechnical Earthquake Engineering, Prentice Hall, New Jersey, 653 pp.

Lin, J. S., & Whitman, R. V. (1983). Decoupling approximation to the evaluation of earthquake-induced plastic slip in earth dams. Earthquake engineering & structural dynamics, 11(5), 667-678.

Makdisi, F. I., & Seed, H. B. (1978). Simplified procedure for estimating dam and embankment earthquake-induced deformations. Journal of Geotechnical and Geoenvironmental Engineering, 104, 849-867

Martha, T. R., Roy, P., Mazumdar, R., Govindharaj, K. B., & Kumar, K. V. (2017). Spatial characteristics of landslides triggered by the 2015 M w 7.8 (Gorkha) and Mw 7.3 (Dolakha) earthquakes in Nepal. Landslides, 14(2), 697-704.

Newmark, N. M. (1965). Effects of earthquakes on dams andembankments. Geotechnique, 15(2), 139-160.

PEER. Next Generation Attenuation West 2 Database. https://ngawest2.berkeley.edu/

Peterman, B. R., & Rathje, E. M. (2016). Evaluation of Ground Motion Selection Techniques for Seismic Rigid Sliding Block Analyses. Journal of Geotechnical and Geoenvironmental Engineering, 143(4).

Plaxis, B. (2016). Reference manual for PLAXIS 2D. Delft, Netherlands: Plaxis.

Plaxis, B. (2016). Material Models manual for PLAXIS 2D. Delft, Netherlands: Plaxis.

Rathje, E. M., & Bray, J. D. (2001). One-and two-dimensional seismic analysis of solid-waste landfills. Canadian Geotechnical Journal, 38(4), 850-862.

Refice, A., & Capolongo, D. (2002). Probabilistic modeling of uncertainties in earthquake-induced landslide hazard assessment. Computers & Geosciences, 28(6), 735-749.

Saygili, G., & Rathje, E. M. (2008). Empirical predictive models for earthquake-induced sliding displacements of slopes. Journal of Geotechnical and Geoenvironmental Engineering, 134(6), 790-803.

Seed, H. B., Lee, K. L., Idriss, I. M., & Makdisi, F. (1973). Analysis of the slides in the San Fernando dams during the earthquake of Feb. 9, 1971. College of Engineering, University of California.

SPSS (IBM Corp. Released 2013. IBM SPSS Statistics for Windows, Version 22.0. Armonk, NY: IBM Corp.).

Spyrakos, C. C., Maniatakis, C. A., & Koutromanos, I. A. (2009). Soil–structure interaction effects on base-isolated buildings founded on soil stratum. Engineering Structures, 31(3), 729-737.

Stewart, J. P., Blake, T. F., & Hollingsworth, R. A. (2003). A screen analysis procedure for seismic slope stability. Earthquake Spectra, 19(3), 697-712.

Strenk, P. M., & Wartman, J. (2011). Uncertainty in seismic slope deformation model predictions. Engineering Geology, 122(1-2), 61-72.

Stroud, M. A. (1988). The standard penetration test–its application and prediction. In Proceedings of the geotechnology conference ‘penetration testing in the UK, Thomas Telford, London

Tanyas, H. (2019). Rapid assessment of earthquake induced landslides.

Terzaghi, K., Peck, R. B., & Mesri, G. (1996). Soil mechanics in engineering practice. John Wiley & Sons.

Terzhagi, K., 1950. Mechanism of landslides. In: Paige, S. (Ed.), Application of Geology to Engineering Practice (Berkey Volume). Geological Society of America, New York, NY, 83–123.

Vucetic, M., & Dobry, R. (1991). Effect of soil plasticity on cyclic response. Journal of geotechnical engineering, 117(1), 89-107.

Watson-Lamprey, J., & Abrahamson, N. (2006). Selection of ground motion time series and limits on scaling. Soil Dynamics and Earthquake Engineering, 26(5), 477-482.

Wilson, R. (1985). Predicting Areal Limit of Earthquake-Induced Landsliding, Evaluating Eathquake Hazards in the Los Angeles Region-An Earth-Science Perspective. US Geological Survery Professional Paper 1360, 317-345.

Xu, R., & Fatahi, B. (2018). Geosynthetic-reinforced cushioned piles with controlled rocking for seismic safeguarding. Geosynthetics International, 25(6), 561-581.